



Out-of-plane capacity of cladding panel-to-structure connections in one-story R/C precast structures

Giovanni Menichini¹ · Emanuele Del Monte^{1,2} · Maurizio Orlando¹ · Andrea Vignoli^{1,2}

Received: 14 April 2020 / Accepted: 16 September 2020
© The Author(s) 2020

Abstract

The interaction between cladding panels and the main structure is a crucial point to assess the seismic response, and above all the structural safety, of RC precast industrial building. In the past, connections were often designed to allow construction tolerances and to accommodate both thermal and wind-induced displacements. The lack of specific details to allow relative in-plane displacements between cladding panels and the main structure often led to the participation of cladding panels in the structure seismic-resistant system with consequent connection failures. In the last decades, a lot of experimental tests were performed to investigate the in-plane performance of panel connections, and some design recommendations have been developed accordingly. In the out-of-plane direction, the connections were often considered to be infinitely rigid and not to suffer any damage by the seismic load. This work deals with the out-of-plane response of panel-to-structure connections for vertical panels typical of industrial and commercial precast buildings. Both standard hammer-head strap and new devices, called SismoSafe, were investigated. Tests were performed in the Structures and Materials Testing Laboratory of the Department of Civil and Environmental Engineering of Florence, where a specific setup was designed to perform cyclic and monotonic tests on the connection devices. Standard connections showed a rather limited resistance, while the innovative connections exhibited a high out-of-plane resistance. Numerical analyses were also performed on a case study building to evaluate the distribution of the out-of-plane demand on the connections.

Keywords Precast structures · Panel-structure connection · Experimental tests · Out-of-plane connection capacity · Nonlinear dynamic analysis

✉ Giovanni Menichini
giovanni.menichini@unifi.it

¹ Dipartimento di Ingegneria Civile e Ambientale, Via di S. Marta 3, 50139 Florence, Italy

² S2R, Spin-Off of University of Florence, Via Vittorio Emanuele II 161, 50134 Florence, Italy

1 Introduction

In Italy and in general, in southern Europe, most of one-story industrial buildings have a precast RC structure. Precast concrete systems are widely used because of short assembly times, lower costs compared to cast on-site buildings and high-quality material standards. The load-bearing structural system of one-story precast structures consists of cantilevered columns and longitudinal beams pinned to the columns. Beams mainly support prestressed roof elements, that span in the transversal direction. One-story precast structures are generally characterized by greater inter-story heights and consequently by larger flexibility than the site-cast buildings. The high lateral flexibility makes the compatibility of displacements between structural and non-structural elements one of the most important aspects that should not be underestimated. The cladding system is generally made of external heavy RC precast panels, which could be vertical or horizontal. In the first case, panels extend from the ground to the roof without intermediate supports. In the second case, panels extend from column to column and they are placed one above the other to fill the entire height of the building.

From the seismic point of view, it is important to know how and if cladding panels interact with the structure.

The panel-to-structure interaction has been studied within many researches: Arnold (1989) and Goodno and Craig (1989) studied cladding systems typical of the United States, while European systems have been extensively studied, among the others, by Baird et al. (2011), Brunesi et al. (2015), Magliulo et al. (2015).

Connection devices can be classified according to the proposal of Biondini et al. (2013) based on the type of panel-to-structure connection into isostatic, integrated and dissipative systems. In the isostatic system, connection devices theoretically detach panels from the structural system; this system includes all those connection systems which, under seismic actions, allow in-plane relative displacements between the structure and panels. In the integrated system, connection devices allow the structure and panels to interact, so the panels should be considered as part of the seismic-resistant system of the building. Finally, the dissipative system concerns those connection devices which are designed as the main source of energy dissipation during earthquakes.

In the past, connections were designed to allow construction tolerances and to accommodate both thermal deformations and displacements induced by wind loads. The lack of specific details to allow displacements and rotations due to a seismic event often led to the involuntary participation of cladding panels in the structure seismic-resistant system with consequent connection failures as highlighted by past seismic events, where several horizontal cladding panels fell down causing danger to people both inside and outside the building and also during evacuation procedures (Toniolo and Colombo (2012), Liberatore et al. (2013), Fischinger et al. (2014), Magliulo et al. (2014)).

Various experimental studies were then conducted on cladding panel connections typically used in industrial buildings within Europe and large-scale pseudo-dynamic tests were conducted on sub-assembly specimens. Experimental investigations were mainly devoted to assessing the in-plane connection behavior.

Concerning the out-of-plane behavior of the connections, the following researches can be reminded: Zoubek et al. (2016) investigated the performance of sliding connections, consisting of two anchor channels connected by hammer-head straps and subjected to a static out-of-plane load; Belleri et al. (2018) illustrated a method to assess the out-of-plane capacity of horizontal panel-structure connections; Dal Lago et al. (2018) experimentally

investigated the in-plane and out-of-plane capacity of a dissipative connector device for the safe fastening of horizontal cladding panels. The out-of-plane behavior of shallow embedded anchors used in panel-to-foundation connections was investigated by Burley et al. (2014), and the experimental campaign was expanded and concluded by Burridge et al. (2015).

A device to prevent the cladding panels from out-of-plane rotation is the so-called “second-line back-up system”, which consists of special anchoring elements and a rope restrainer (Zoubek et al. (2018).

From previous experimental campaigns, some design recommendations were derived (Colombo et al. 2016), mainly concerning the in-plane behavior of panel-to-structure connections. For out-of-plane loading, the seismic demand on elements and connections for the cladding system is expressed in terms of forces instead of displacements. The demand is usually determined following formulas of the construction code for non-structural elements (EN EN 1998-1, 2005).

This work aims at studying the out-of-plane response of panel-to-structure connections for vertical panels typical of industrial and commercial precast buildings. Both standard hammer-head strap connections and a new device, called SismoSafe (Del Monte et al. 2019), were tested for out-of-plane loads, without considering the interaction with the in-plane response, which could significantly modify the out-of-plane capacity of the connections under investigation. As a matter of fact, in-use devices, like hammer-head steel straps, could be seriously damaged due to in-plane seismic loads, even if they were designed to uncouple the relative in-plane displacements between the panels and the structure, while the new SismoSafe devices are substantially undamaged for in-plane seismic loads (Del Monte et al. 2019). Therefore, the out-of-plane capacity of standard devices was overestimated, because the in-plane damage was neglected in the experimental campaign, while experimental results for the new type of devices could be thought to be accurate, as they do not undergo in-plane damage.

2 Experimental campaign

An experimental campaign was carried out on panel-to-structure connections of the isotatic system type for vertical cladding panels. All tests were executed at the Structures and Materials Testing Laboratory of the Department of Civil and Environmental Engineering of the University of Florence.

2.1 Types of connection devices

Both in-use commercial connection devices (called Standard in the following) and innovative SismoSafe devices were tested. The Standard device consists of a hammer-head steel strap, a hammer-head bolt, and two anchor channels, which are pre-installed in both the panel and the beam. The strap is fastened to the channel on the beam side by means of a hammer-head bolt and the strap’s head is fixed inside the channel on the panel side (Fig. 1a).

The SismoSafe device consists of two vertical anchor channel profiles fixed on the panel before it is cast; a skid, to which a mobile guide rail is welded, can slide vertically inside the two channels. The profile of the mobile guide rail is installed on a fixed guide rail, which in turn is fixed to the beam through two self-tapping screws (Fig. 1b).

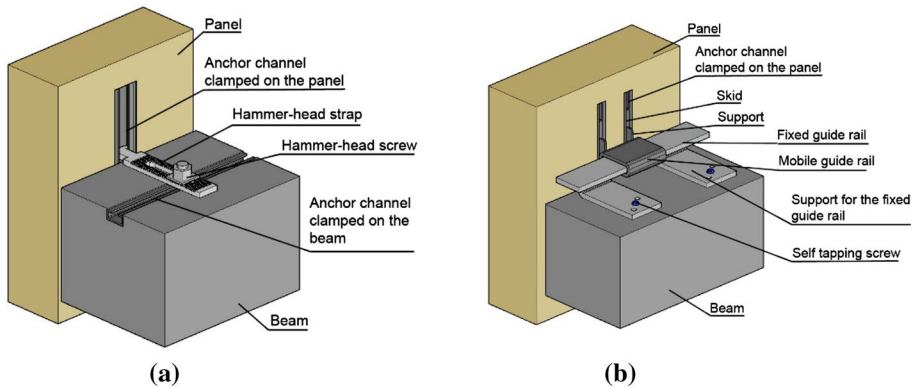


Fig. 1 The hammer-head strap connection (a) and the SismoSafe connection (b)

2.2 Design and aim of tests

During a seismic event, panel-to-structure connections should accommodate relative displacements between panels and the main structure, but they should also support out-of-plane forces. In the design phase, these connections are generally considered to be rigid in the out-of-plane direction, along with they are dimensioned considering their resistance capacity. To assess the out-of-plane resistance capacity of both Standard and SismoSafe devices, a series of tests were carried out.

The experimental campaign consisted of 30 tests: 6 tests were performed on Standard devices and 24 tests on SismoSafe devices. The large number of tests on SismoSafe devices was needed to identify a suitable geometry, with special attention to the curvature of the fixed guide rail supports and the welding length, to avoid the brittle failure of devices. In the present paper, only the 6 tests on devices with the final geometry are illustrated and discussed. For each type, both monotonic and cyclic load time-histories were considered. Tests differed for the following two aspects:

- Type of device. Standard or SismoSafe
- Side of the connection. For each device, both the connection to the cladding panel and the connection to the beam were tested.

Table 1 lists the six tests on Standard devices and the six tests on SismoSafe devices with the final geometry. The designation of each test has been chosen to easily identify the

Table 1 Summary of tests

Number of tests	Test designation	Connection side	Type of device
3	P_St_M1, P_St_C1, P_St_C2	Panel	Standard
3	B_St_M1, B_St_C1, B_St_C2	Beam	Standard
3	P_Sismo_M1, P_Sismo_C1, P_Sismo_C2	Panel	SismoSafe®
3	B_Sismo_M1, B_Sismo_M2, B_Sismo_C1	Beam	SismoSafe®

connection tested (“P” for panel connection, “B” for beam connection), the type of device (“St” for Standard device, “Sismo” for SismoSafe device) and the loading type (“M” for monotonic loading, “C” for cyclic loading); moreover, a digit (1 or 2) identifies the first or the second test performed on the same connection under the same input motion type, monotonic or cyclic.

2.3 Experimental setup

The test setup consists of the following elements (Fig. 2):

- the specimen (RC beam or panel) suitably equipped with channel profiles to host the connection device;
- a hydraulic jack;
- a steel sleeve to join the tested device to the hydraulic jack;
- a load cell mounted on the hydraulic jack.

Each panel or beam specimen was fixed to the testing apparatus, which was formed by an MTS machine with a loading capacity of 500 kN. The hydraulic jack was placed closer to the specimen, as the crosshead could be moved up and down by lowering or lifting the extendable columns. All tests were performed under displacement control.

2.4 Experimental tests

To evaluate the maximum capacity of connections, both monotonic (Fig. 3a) and cyclic (Fig. 3b) tests were performed under displacement control. The cyclic tests consisted of

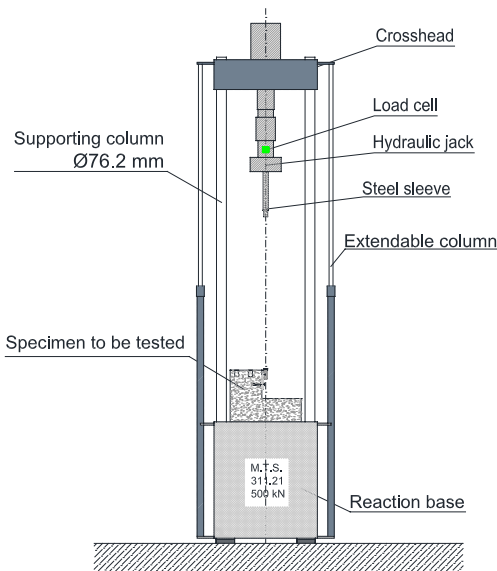


Fig. 2 M.T.S. 311.21 testing apparatus

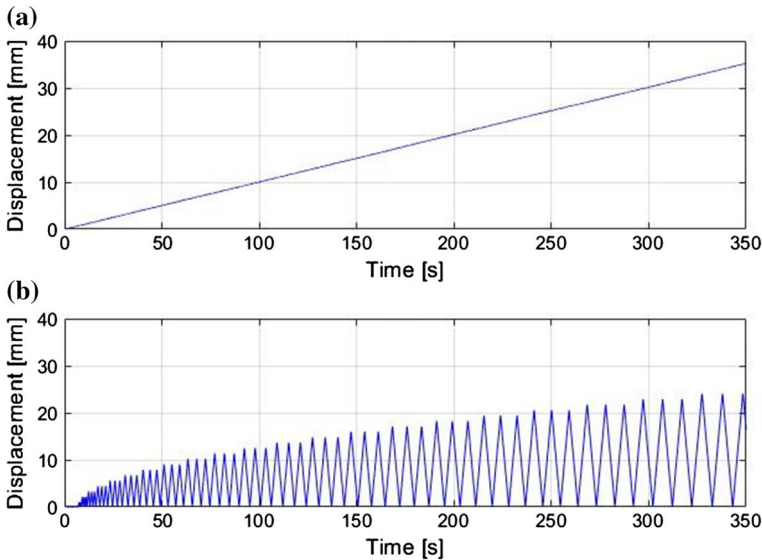


Fig. 3 Applied displacement history: constant increasing displacement (a) and three cycles of increasing amplitude (b)

groups of three cycles of the same amplitude, with subsequent increment Δd between two successive groups up to the ultimate connection capacity. The amplitude d_1 of the first group was taken as $1/20$ of the maximum expected displacement; the amplitude increment Δd from one group of cycles to the subsequent group was taken equal to d_1 .

In the cyclic displacement history, the amplitude d_1 of the first group, as well as the increase Δd between one cycle and the next, was assumed equal to 1 mm. For monotonic tests, a very low relative velocity of 0.1 mm/s was used to exclude as much as possible dynamic effects, while during cyclic tests a value of 5 mm/s was chosen as it is of the same order of magnitude of the maximum relative velocity registered in real one-story precast buildings under medium seismic excitation. The adopted value of 5 mm/s is also close to the relative velocities between cladding panels and the main structure provided by the numerical model of the case study presented within this work for different seismic inputs. Figure 4 shows the specimens of a Standard connection ready for the test, while Fig. 5 shows the specimens of a SismoSafe connection.

For the panel connection of Standard devices, the hammer-head strap, provided with a welded end bolt fixed to the testing apparatus, was inserted in an anchor channel pre-installed on the panel specimen (Fig. 6a). For the beam connection of Standard devices, the hammer-head strap was fixed to the testing apparatus by means of a bolt welded on the hammer-head side. On the other side, the strap was fastened to the beam specimen through a hammer-head bolt which was inserted into a channel profile previously installed on the beam. The hammer-head bolt was provided with a slide to prevent the locking in the channel profile (Fig. 6b).

Concerning the test setup for panel connections of SismoSafe devices, the mobile guide was mounted on the panel specimen by inserting the two skids in the pre-installed anchor channel profiles, and the mobile guide had a welded bolt that was screwed into the test apparatus connection sleeve (Fig. 7a).

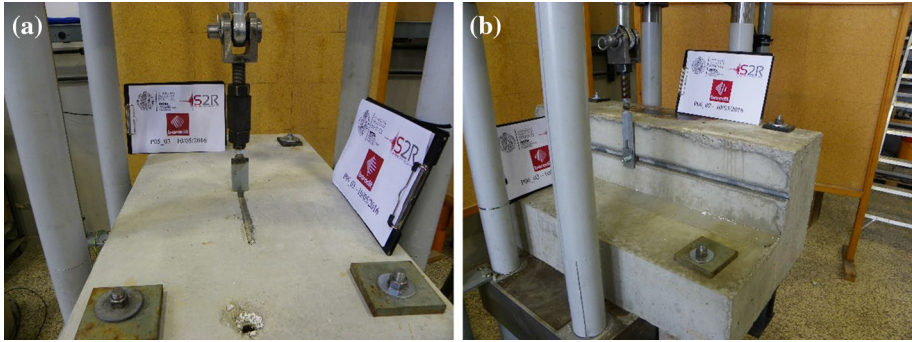


Fig. 4 Experimental test setup: P_St_M1 (a) and B_St_M1 (b)

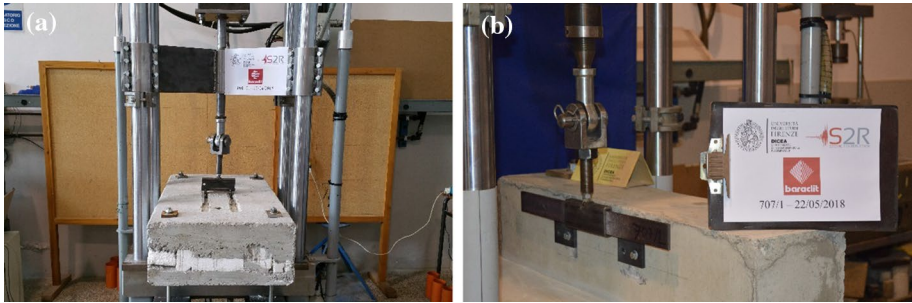


Fig. 5 Experimental test setup: P_Sismo_C1 (a) and B_Sismo_M1 (b)

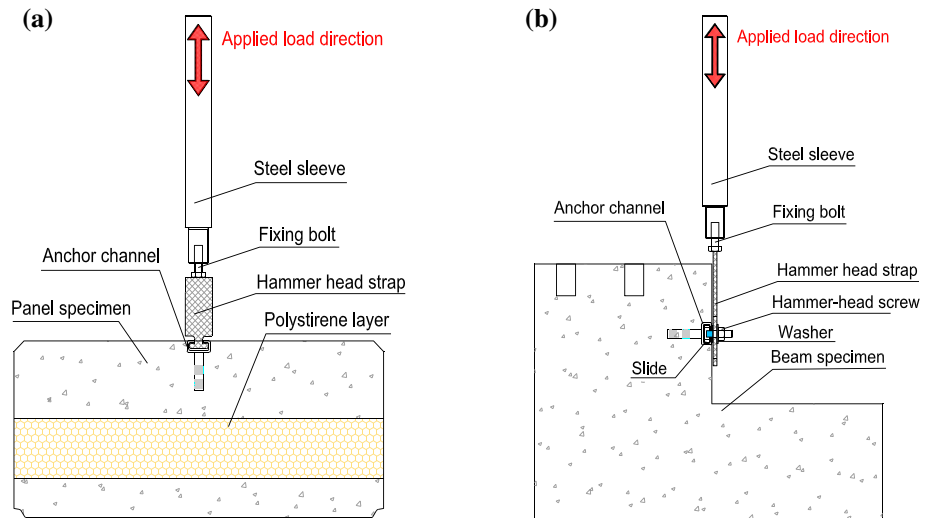


Fig. 6 Layout test of a Standard connection for vertical panels to evaluate the resistance on the panel side (a) and on the beam side (b)

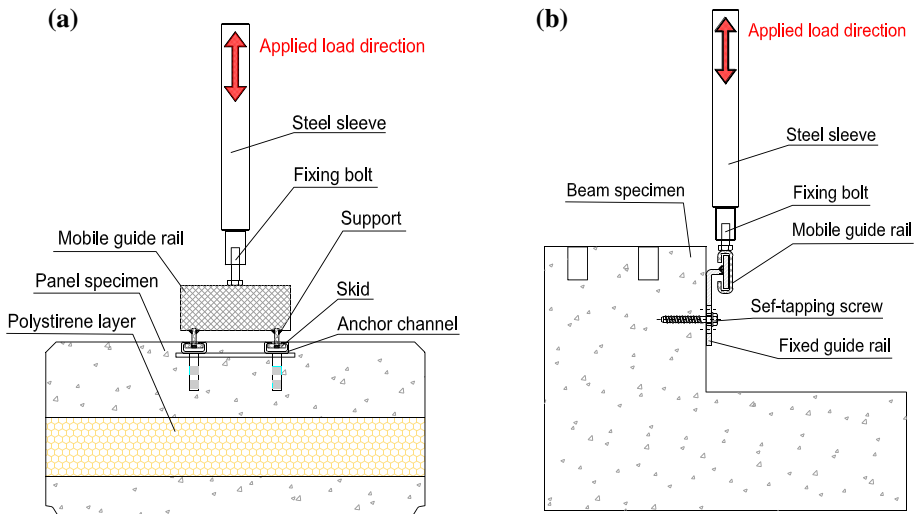


Fig. 7 Layout test of a SismoSafe connection for vertical panels to evaluate the resistance on the panel side (a) and on the beam side (b)

For beam connections, the fixed guide was installed on the beam specimen by means of two self-tapping screws. Then the mobile guide was mounted on the fixed guide. The mobile guide was provided with a welded bolt to fix onto the test equipment (Fig. 7b).

2.4.1 Experimental results

Standard devices showed initially a quite stiff behavior on the panel side: the stiffness was about 3500 kN/m (Fig. 8a). During the monotonic test (P_St_M1), some cracks started to appear on the concrete around the fixing point of the steel strap at the displacement of 3–4 mm. As the imposed displacement increases, cracks become wider until the complete detachment of the concrete surface layer (about 10 mm). Then, the channel profile began to bend upwards until the head of the steel strap opens the edges of the anchor channel profile (Fig. 8b). During the cyclic test (P_St_C1 and P_St_C2) initially a rather rigid elastic branch was observed. By increasing the amplitude of the cyclic displacement some cracks began to appear around the channel profile, gradually extending along the whole length. Later, the concrete surface layer (about 10 mm) detached and the channel profile was bent, alternately upwards and downwards, by the cyclic load. Finally, the channel profile was detached from the concrete due to the failure of its fastening clamps (Fig. 8c, d).

The maximum values of forces and displacements of each test are listed in Table 2.

The beam connection also exhibited a rather rigid elastic behavior, the stiffness was approximately equal to 4000 kN/m (Fig. 9a). During the monotonic test (B_St_M1), the displacement of 1–2 mm, some semi-circular cracks started to appear on the concrete around the fixing point of the steel strap. With the increase of the imposed displacement, the strap began to bend around the hammer-head fixing bolt. The inflexion became larger and larger below the bolt washer until the slide pushed against the anchor channel edge, opening it and detaching the steel strap from the beam (Fig. 9b).

In the cyclic test (B_st_C1 and B_st_C2) the behavior is similar to the monotonic test with the formation of semi-circular cracks on the concrete around the hammer fixing

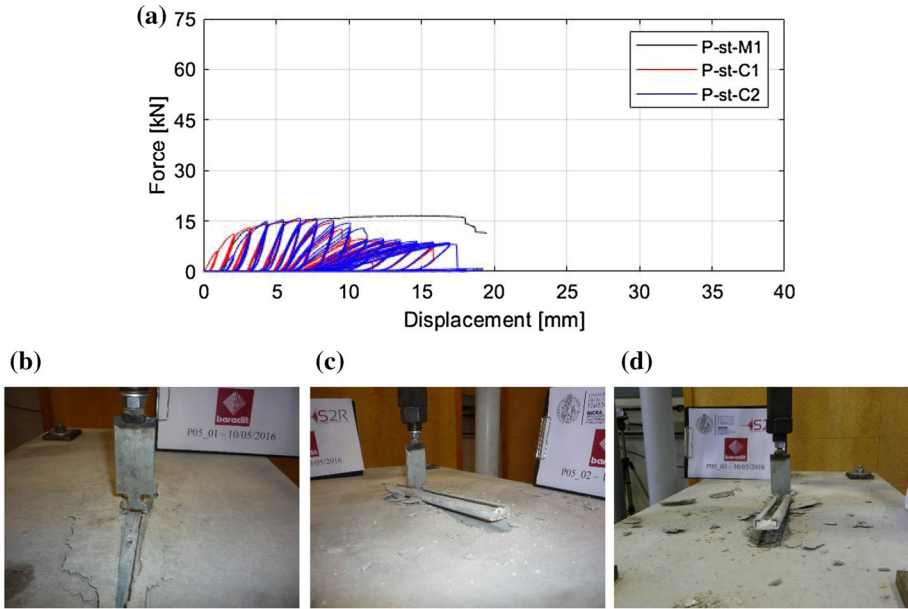


Fig. 8 Standard connection test on panel side: force–displacement relationship (a) anchor channel edge failure in monotonic test P_St_M1 (b). Anchor channel clamps failure in cyclic test P_St_C1 (c) and P_St_C2 (d)

Table 2 Maximum values for P_St_M, P_St_C1 and C2 tests

Test label	Displ. time history	F _{max} (kN)	d _{max} (mm)
P_St_M1	Monotonic	16.62	14.21
P_St_C1	Cyclic	15.22	6.57
P_St_C2	Cyclic	15.84	6.59

bolt on the channel profile. The cyclic load effect caused the anti-lock slide to push against both edges of the channel profile, opening them and causing the slide to break into two parts. The steel strap was thus detached from the beam (Fig. 9c, d).

The maximum values of forces and displacements for each test are listed in Table 3.

The SismoSafe device showed on the panel connection a stiffer behavior than the Standard type, as the stiffness was equal to 9830 kN/m, about 2.8 times higher (Fig. 10a). During the monotonic test (P_Sismo_M1), after the elastic phase, some cracks started to arise on the concrete between the two anchor channels in the transversal direction. Cracks developed from the point where the two slides of the mobile guide rail were inserted into the channel profile, when the displacement increased, cracks also developed outside the two anchor channel profiles. Later, the welding between the fixing clamps and the channel profile reached the failure. The anchor channels were lifted upwards by the applied force and were progressively detached from the panel (Fig. 10b).

In the cyclic tests (P_Sismo_C1 and P_Sismo_C2) the behavior was completely like the monotonic test with the formation of cracks in the concrete around the fixing skirts of the mobile guide. The load cyclic effect bent the two anchor channel profiles upwards and

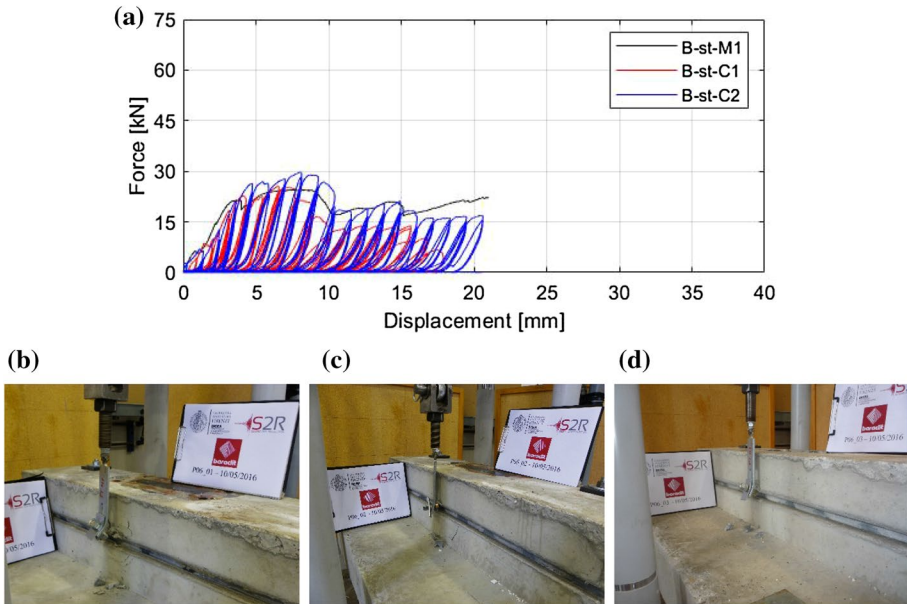


Fig. 9 Standard connection test on the beam side: force–displacement relationship (a) anchor channel edge failure in monotonic test B_St_M1 (b). Anchor channel opening and slide failure in cyclic test B_St_C1 (c) and B_St_C2 (d)

Table 3 Maximum values for B_St_M, B_St_C1 and C2 tests

Test label	Displ. time history	F_{\max} (kN)	d_{\max} (mm)
B_St_M1	Monotonic	24.64	7.47
B_St_C1	Cyclic	25.60	6.55
B_St_C2	Cyclic	29.80	9.88

downwards causing the welding failure between the fixing clamps and the channel profile. Finally, both anchor channels were torn off from the concrete (Fig. 10c, d).

The maximum values of forces and displacements for each test are listed in Table 4. It is worth noting that the maximum force values are about three times higher than Standard devices (see Table 2).

The beam connection of the SismoSafe devices was more rigid than the panel connection (about 11,775 kN/m), as shown in Fig. 11a.

During the monotonic test (B_Sismo_M1 and B_Sismo_M2), no crack developed in the concrete not even around the self-tapping fixing screws. The fixed guide rail was dragged by the displacement imposed on the mobile guide rail and it was bent upwards. As the displacement increased, it was possible to observe an opening of the edges of the mobile guide rail. Due to its increasing opening, in the end, the mobile guide rail was slipped out from the fixed guide (Fig. 11b). In the cyclic test (B_Sismo_C1) the behavior was the same as the monotonic test. The cyclic effect of the load caused the fixed guide to bend both downwards and upwards and the failure occurred due to the bending of the bolt fixing the mobile guide rail to the test apparatus (Fig. 11c, d).

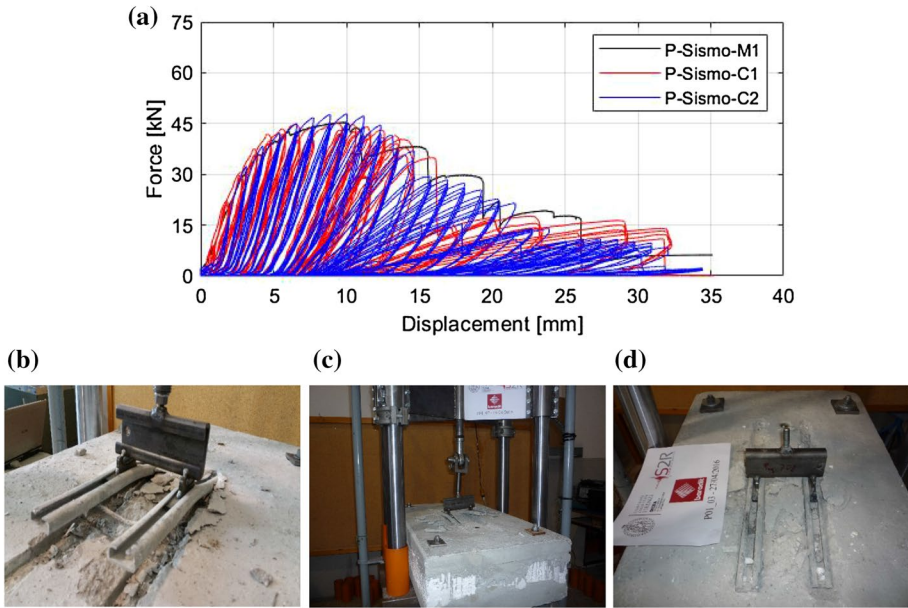


Fig. 10 SismoSafe connection test on the panel side: force–displacement relationship (a) anchor channel clamps failure in monotonic test P_Sismo_M1 (b). Anchor channel clamps failure in cyclic test P_Sismo_C1 (c) and P_Sismo_C2 (d)

Table 4 Maximum values for P_Sismo_M1, P_Sismo_C1 and C2 tests

Test label	Displ. time history	F_{max} (kN)	d_{max} (mm)
P_Sismo_M1	Monotonic	45.42	10.57
P_Sismo_C1	Cyclic	45.16	9.84
P_Sismo_C2	Cyclic	47.84	11.31

The maximum values of forces and displacements for each test are listed in Table 5.

The maximum force values are about double times higher than Standard devices (see Table 3).

3 Case study

A case study is presented to investigate the seismic behavior of SismoSafe connections in a one-story precast industrial building. The study is aimed at understanding the distribution of out-of-plane seismic forces on SismoSafe connections. The interaction between the cladding panels and the main structure is investigated considering the in-plane friction forces transmitted by the connections or neglecting the friction. The four among the strongest seismic events which struck the Italian territory in the last 12 years and caused significant damage to the RC precast structures were considered in the numerical analysis (Ercolino et al. 2016; Savoia et al. 2017).

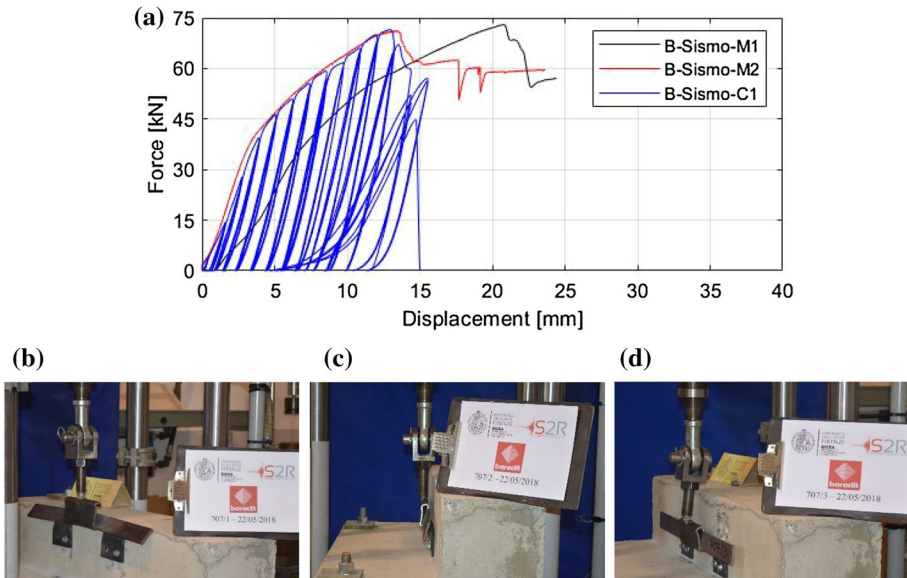


Fig. 11 Test on a SismoSafe beam connection: force–displacement relationship (a) fixed guide upward bending (b) mobile guide edge opening (c) and fixing bolt deflection (d)

Table 5 Maximum values for B_Sismo_M1, B_Sismo_M2 and C1 tests

Test label	Displ. time history	F_{\max} (kN)	d_{\max} (mm)
B_Sismo_M1	Monotonic	72.96	20.76
B_Sismo_M2	Monotonic	71.27	13.86
B_Sismo_C1	Cyclic	71.50	13.42

3.1 Building geometry

The case study of an industrial building with a $69.36 \text{ m} \times 36.62 \text{ m}$ rectangular plan is considered (Fig. 12). It is made of precast RC columns and beams, prestressed RC roofing beams and vertical RC cladding panels.

Columns are 10.30 m high, while vertical cladding panels are 11.40 m high, so they cover the roof elements, as shown in the front views of the building in Fig. 12. The building was designed according to Eurocode 2 (EN 1992-1-1, 2004) and Eurocode 8 (EN 1998-1-1, 2005) adopting C40/50 grade concrete and S500 steel grade with ductility class C for reinforcing bars.

The dead weight of roof elements is equal to 0.93 kN/m^2 , while the secondary roof elements have a dead weight of 0.1 kN/m^2 ; moreover, a super dead load due to electrical/hydraulic systems of 0.11 kN/m^2 is considered.

The cross-sections of the main structural element, with their weight per unit length, are described in Fig. 13, which also reports the material characteristics.

The RC columns are fixed at the base in socketed footings; at the top, they are connected to the beams through pinned connections. The vertical cladding panels, at the base, are hinged in the out-of-plane direction and fully restrained in their plane. At the top, they are connected to the beams with SismoSafe devices shown in the previous Fig. 1b.

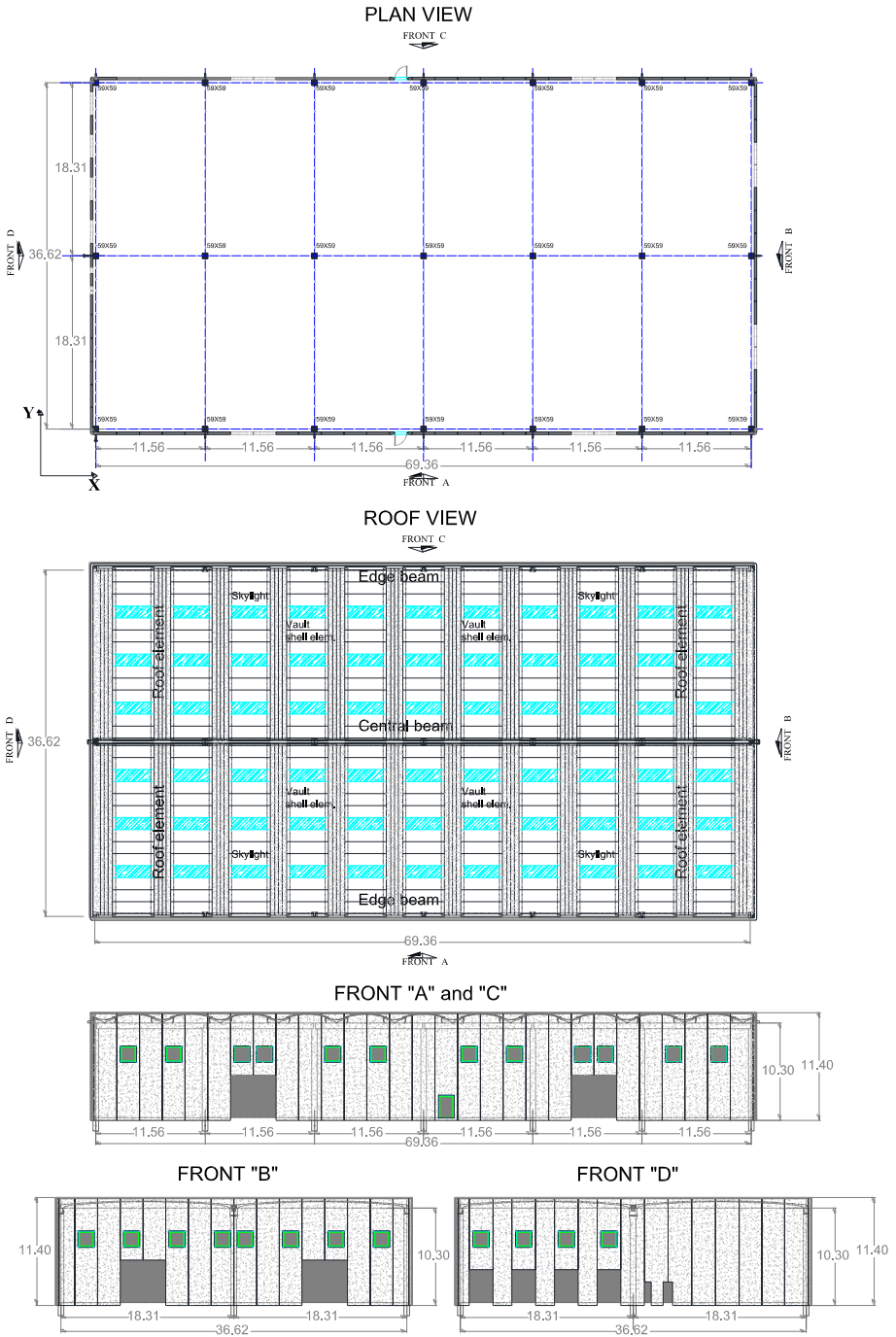
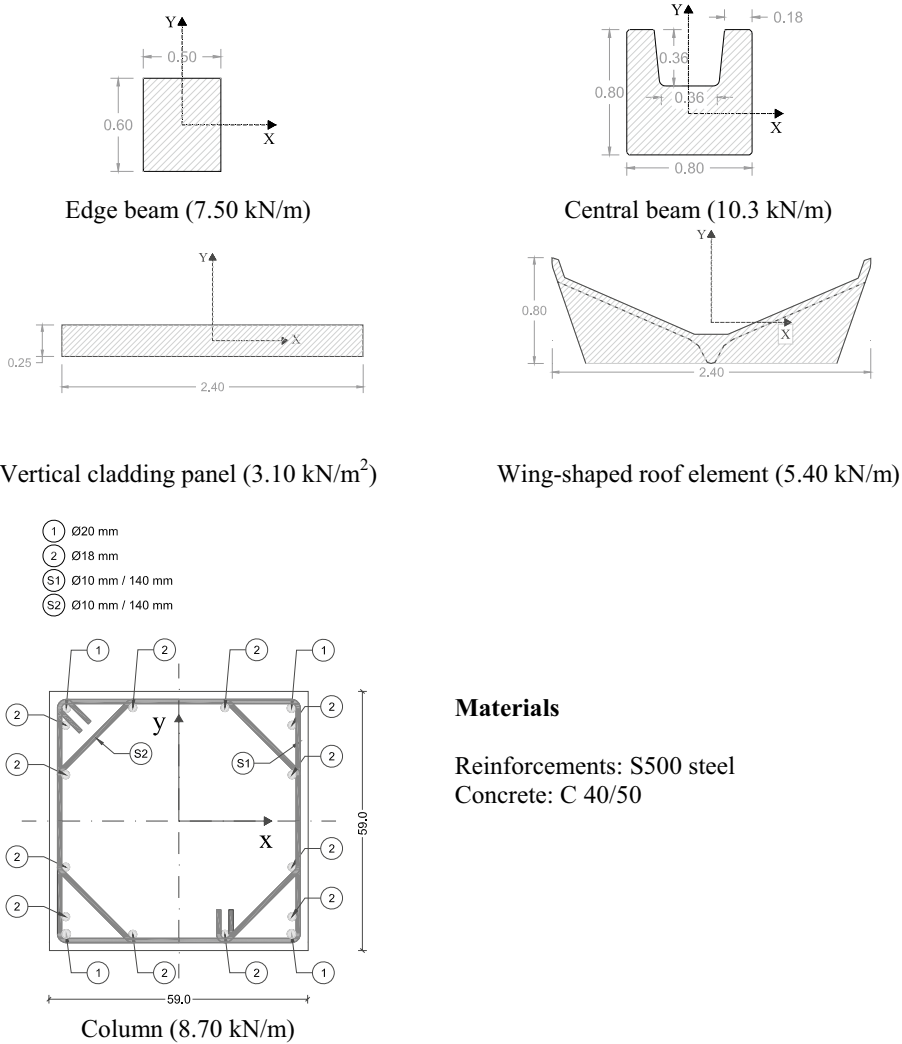


Fig. 12 Building plan and front views



Materials

Reinforcements: S500 steel
 Concrete: C 40/50

Fig. 13 Cross-sections of main structural elements with their weight per unit length

Each end of the roof-beam is placed on a cast-in situ mortar bed and connected to the main beam through two steel angle plates, one on each side of the end section. Each angle plate is fixed to the main beam through a hammer-head bolt, inserted in an anchor channel profile, so that its positioning is adjustable, while the angle plate is fixed to the roof beam through a fixing bolt (Fig. 14).

The two connections not only prevent the relative horizontal displacement between the end section of the roof beam and the main beam, but also the relative rotation in the horizontal plane, through the transmission of a couple of shear forces; according to Belletti et al. (2015), the connection can be defined as a static indeterminate connection. Due to the double connection of each end section of the roof beams, under longitudinal seismic loading the relative displacement between the edge frames and the central frame is opposed by the flexural stiffness of the double-fixed roof beams (Fig. 15a), while for transversal seismic loading the

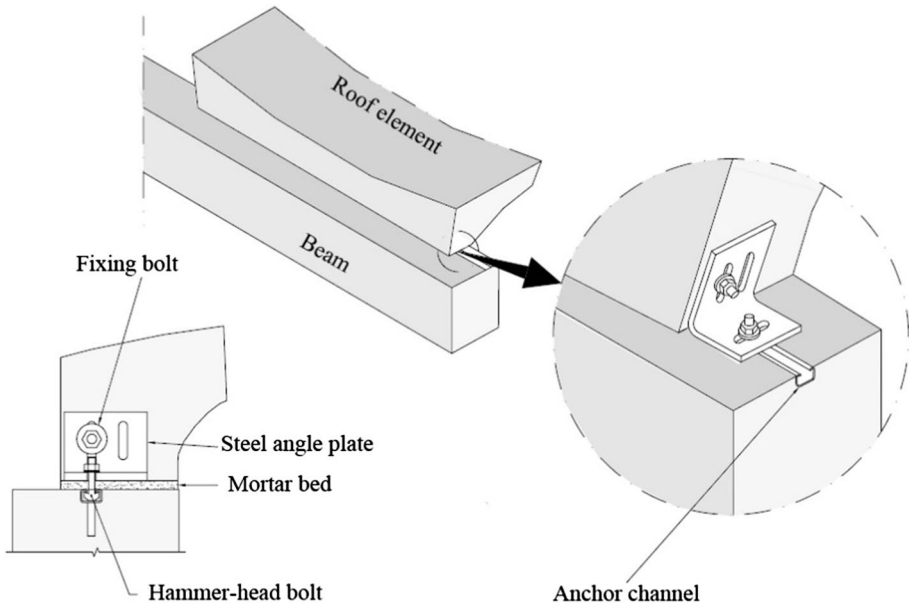


Fig. 14 Beam-roof element connection (Mandelli et al. 2007)

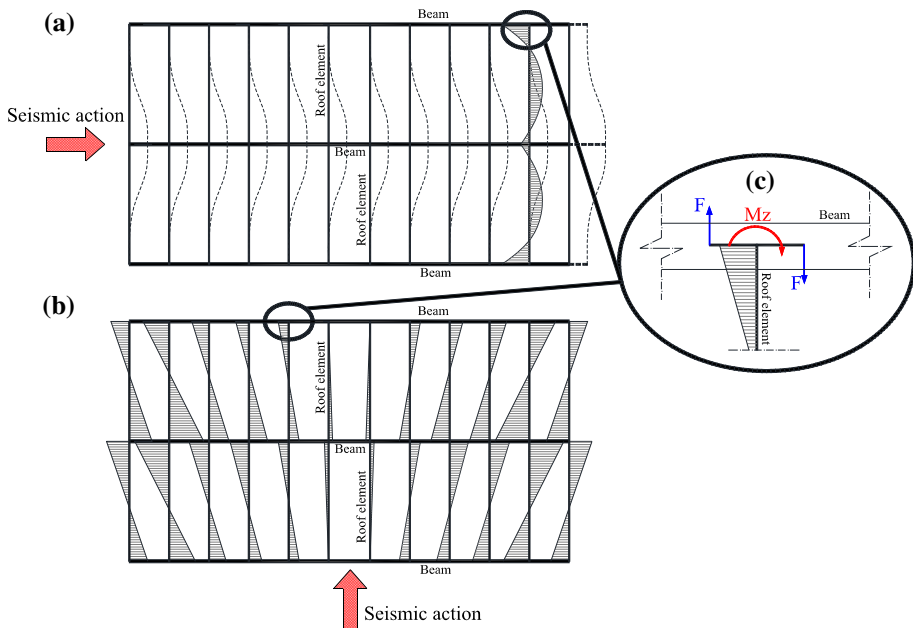


Fig. 15 Bending moment distribution in the roof beams due to longitudinal (a) or transversal (b) seismic loading and horizontal shear forces in the connections (c)

roofing system behaves like a Vierendeel beam (Fig. 15b). IBC (IBC 2018) states that diaphragms are rigid for distribution of story shear and torsional moment when the ratio of the lateral deformation of the diaphragm and the average of the story drift is less than or equal to two. In the present case, considering the strongest among the selected ground motions, the ratio is equal to 0.052 in the longitudinal direction and to 0.116 in the transversal direction, therefore the roof diaphragm can be assumed to be rigid. The high in-plane stiffness of the roof can cause high horizontal shear forces in the roof beam connections under horizontal seismic load (Fig. 15c); nevertheless, in all the numerical analyses, those shear forces never exceeded the resistance of the connections. The presence of a rigid roofing system allows for the seismic loads to be distributed proportionally to the stiffness of the columns, which are subjected to the same shear and bending moment. Therefore, the most vulnerable columns are the four corner columns, which are subjected to the lowest axial forces.

3.2 Numerical model

The numerical model was created using the OpenSees software (Mazzoni et al. 2006). All prismatic elements were modelled with elastic elements, except for the columns, which were modelled using fiber elements since they are the main location of the inelastic behavior of the structure. The non-linear behavior of the column elements is monitored at several control sections (Gauss–Lobatto integration sections) that are, in turn, discretized into longitudinal steel and concrete fibers. The non-linear section behavior, thus, derives from the integration of the non-linear stress–strain behavior of the fibers. The constitutive relationships used in the model for the concrete and steel rebars are illustrated in Fig. 16. For columns, the stirrup confinement effect was considered through the confinement effectiveness factor α provided by Eurocode 8 (EN 1998-1-1, 2005). Considering the column geometry and reinforcements depicted in Fig. 13, α holds 0.63, then the confining pressure σ_2 is equal to 0.95 N/mm^2 and substituting in the expression of $f_{ck,c}$ provided by EN 1992-1-1 (EN 1992-1-1, 2004), the ratio K between the resistance of confined ($f_{ck,c}$) and unconfined (f_{ck}) concrete is equal to $K = f_{ckc}/f_{ck} = 1.1$.

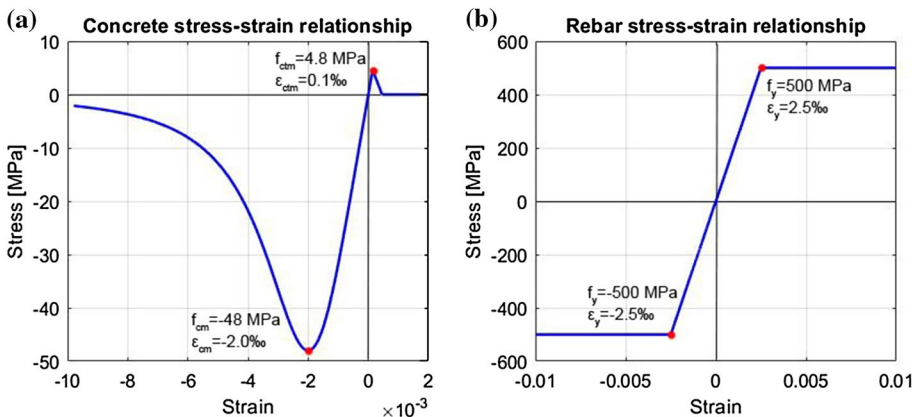


Fig. 16 Mander model (Mander et al. 1988) for concrete (a) and elastic–plastic model for rebar (b)

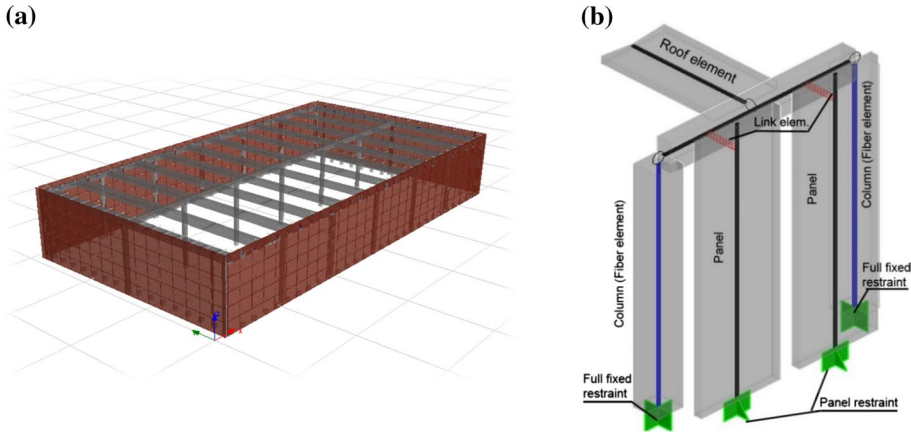


Fig. 17 Numerical model: 3D view (a) and details of non-linear and linear elements assembly (b)

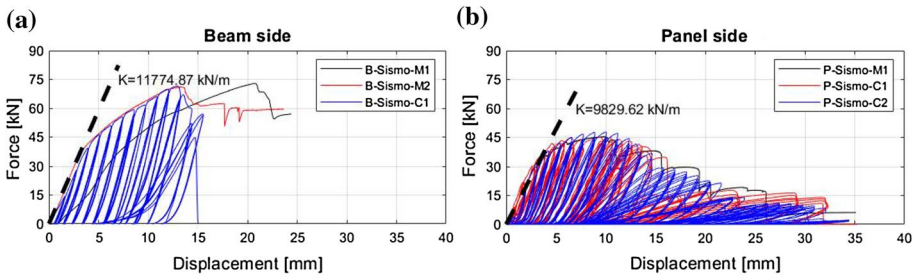


Fig. 18 Tangent elastic stiffness measured during the experimental test on the beam side (a) and on panel side (b)

The SismoSafe panel-to-structure connections are modelled through link elements. At the base, the columns are fully fixed, while the panels are equipped with out-of-plane hinges and are fully restrained in their plane (Fig. 17).

The friction force F_μ generated during the relative sliding between the panel and the structure depends on the out-of-plane force F_c (Fig. 19b):

$$F_\mu(t) = \mu \cdot F_c(t) \tag{1}$$

The *Flat Slider Bearing Element* was used to simulate the frictional behavior. This element requires the definition of a friction model which specifies the behavior of the coefficient of friction in terms of the absolute sliding velocity and the normal pressure on the contact area.

Its axial elastic stiffness was evaluated from the experimental values of the beam connection stiffness and panel connection stiffness (Fig. 18), assuming that the two stiffnesses are in series. As the beam connection stiffness holds 11,775 kN/m and the panel connection stiffness 9830 kN/m, the total axial elastic stiffness holds 5357 kN/m.

The frictional behavior is defined by associating a Coulomb friction model to the horizontal sliding direction (Fig. 19a). In this model, the kinetic friction is independent of the sliding speed.

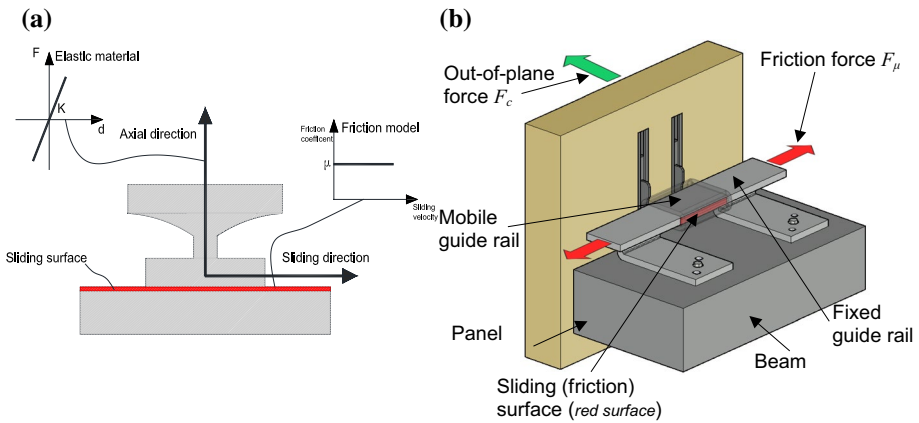


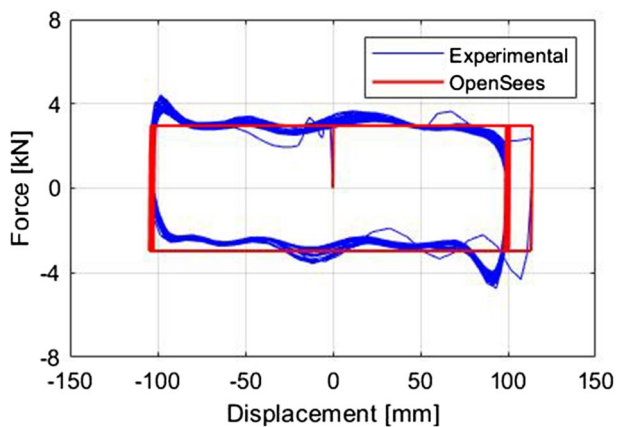
Fig. 19 Flat slider bearing element (a) and sliding surface and direction of friction force in the connection device (b)

Using the same imposed displacement function and the same out-of-plane force of the test F15-04 from Del Monte et al. (2019) and assuming the friction coefficient μ equal to 0.4, the numerical and experimental curves for a single SismoSafe device are in good agreement, as shown in Fig. 20.

The OpenSees numerical model of the whole structure was used to evaluate the out-of-plane force in the connection devices through nonlinear dynamic analyses. Three cases have been studied according to the behavior assigned to the link that connects the panels to the edge beams:

- case 1: the experimental out-of-plane stiffness was assigned to the link element in its axial direction, while the link element was free to move in the in-plane direction,
- case 2: the same as case 1, with the assignment of the friction coefficient $\mu = 0.4$ in the in-plane direction,
- case 3: the same as case 2, with the assumption that the roof behaves like a rigid diaphragm.

Fig. 20 SismoSafe device: comparison between the numerical and experimental curves



3.3 Seismic action

The four strongest earthquakes that stroke the Italian territory in the period between 2009 and 2016 were taken from the ITACA Database (Luzy et al. 2019). The main feature of the chosen unscaled accelerograms are reported in Table 6, where R is the epicentral distance and M_w is the moment magnitude and t_D the record duration.

The acceleration spectrum S_A and the displacement spectrum S_D of the chosen unscaled accelerograms are reported in the Fig. 21.

3.4 Results

Fixed a cartesian reference system (Fig. 22), Figs. 23, 24, 25 and 26 show the graphs of the structure displacements, the chord rotation of the most stressed column, the out-of-plane forces on the connections, the lifting force on the panels and the shear force at the panel bases.

In the graphs of Figs. 23 ÷ 26 the values of X and Y identify the position of the frames arranged in the Y and X direction, respectively. The graphs show the maximum values over time of the studied quantities.

3.5 Discussion of the case study results

3.5.1 Structure displacements

The mean displacement of the structure in the Case 1, where in-plane friction forces in the connections are neglected, is about 65% and 25% greater in the X and Y direction, respectively, compared to the Case 2, where friction at connections is considered (see Figs. 23, 24, 25, 26a, c). The difference is evidently due to the constraint force produced by the friction in the connections. In Table 7, for each case study, each direction of seismic action (X or Y) and each seismic event, the maximum, minimum, mean displacement value and the percentage difference with Case 3, are listed.

For Case 3, since the roof behaves like a rigid diaphragm, the maximum, minimum, mean displacement value are the same and only the latter is reported in Table 7.

Table 6 Accelerograms utilized in nonlinear dynamic analysis

Number	Event name	Station name	Date	PGA (g)	M_w	R (km)	$V_{s,30}$ (m/s)	Duration t_D (s)
1	L'Aquila	AQK	2009-04-06	0.353	6.1	1.8	705	100.00
2	Emilia 1st shock	MRN	2012-05-20	0.263	6.1	16.1	208	130.15
3	Central Italy	NRC	2016-10-30	0.485	6.5	4.6	498	50.00
4	Emilia 2nd shock	MRN	2012-05-29	0.218	6.0	4.1	208	68.00

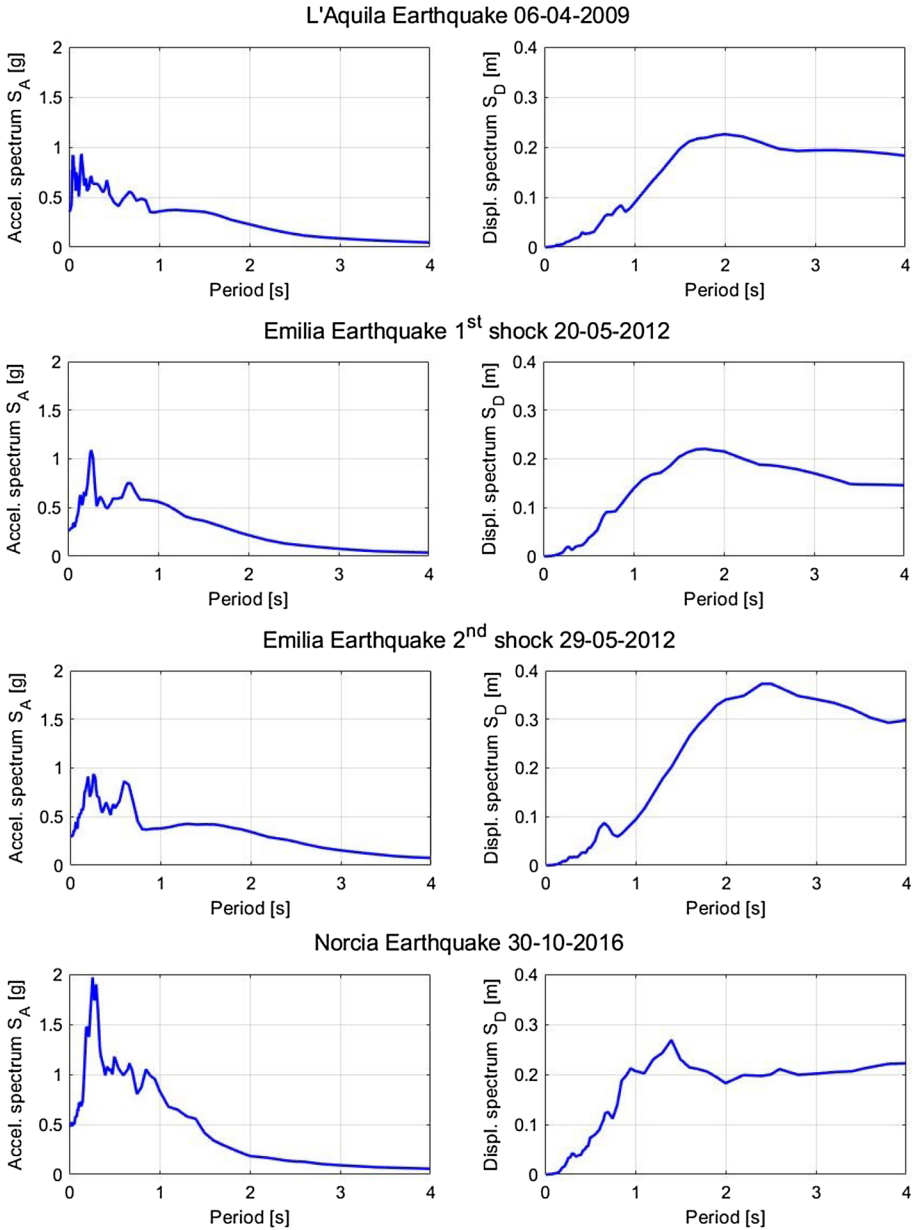


Fig. 21 Spectrum acceleration and displacement for the chosen seismic events

3.5.2 Column chord rotation

In Case 1, where connection friction forces are neglected, the chord rotation demand on the columns exceeds the yielding chord rotation θ_y for all the four seismic events. While, in the Case 2 with the friction in the connections, the chord rotation demand in the columns

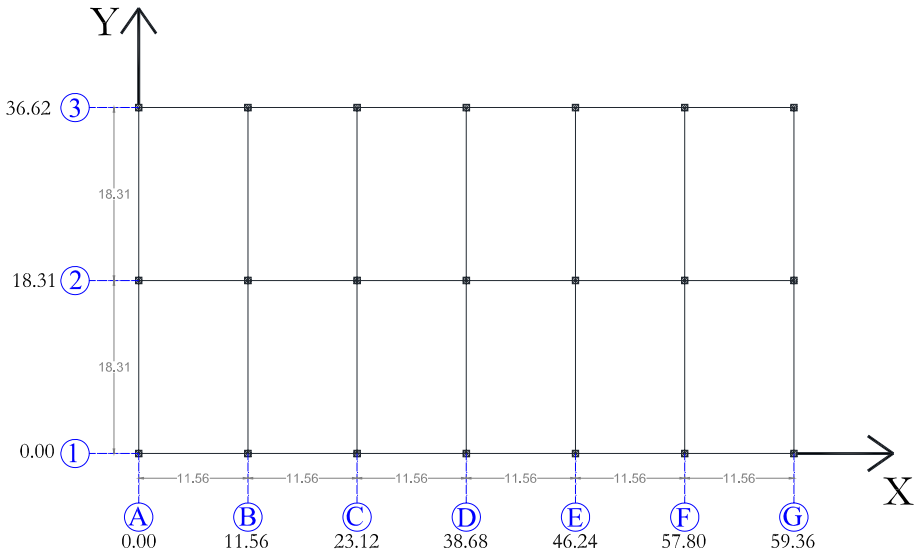


Fig. 22 Wireframe plan view of the building and the coordinate reference system

is lower and the yielding chord rotation θ_y is only achieved for the two most severe seismic events (Norcia and Emilia 2nd shock), as shown in Figs. 23, 24, 25, 26b, d. The chord rotation demand reduction can be positive to preserve the integrity of the columns or some column-foundation mechanical connection devices such as those studied in Dal Lago et al. (2016) and Orlando and Piscitelli (2018).

However, if on one hand, the friction at the connections parallel to the seismic excitation reduces the structure mean displacement and the chord rotation demand in the columns, on the other hand, it increases the in-plane force demand at the base of panels, as depicted in Figs. 23, 24, 25 and 26g, h, i and l. This aspect is discussed in detail in Sect. 3.6.

3.5.3 Connection out-of-plane forces

When the frictional behavior is considered (Case 2) the connection out-of-plane forces increase compared to Case 1 without friction (see Figs. 23, 24, 25, 26e and f). Nevertheless, the demand for out-of-plane forces never exceeds the capacity of the SismoSafe devices, which is equal to 45 kN (§ 2.4.1). Moreover, if the roof system is considered as a rigid diaphragm (Case 3), the out-of-plane forces assume a constant value, which is equal to approximately the mean value of Case 2.

In Table 8, for each case study, each direction of seismic action (X or Y) and each seismic event, the maximum, minimum, mean out-of-plane force value on connections and the percentage difference respect to Case 3, are listed.

For Case 3, since the roof behaves like a rigid diaphragm, the maximum, minimum, mean out-of-plane force are the same and only the latter is reported in Table 8.

The connection out-of-plane forces show both in the X and Y direction a wavy trend: the force is higher in the connections close to the edge frames, especially in Case 2 where the friction is considered. For panels lying in the transversal Y direction, that trend can be explained by schematizing the building as an equivalent transversal beam having the flexural stiffness of the roofing edge transversal beam (A or G in Fig. 27) to

L'Aquila Earthquake Apr. 06, 2009

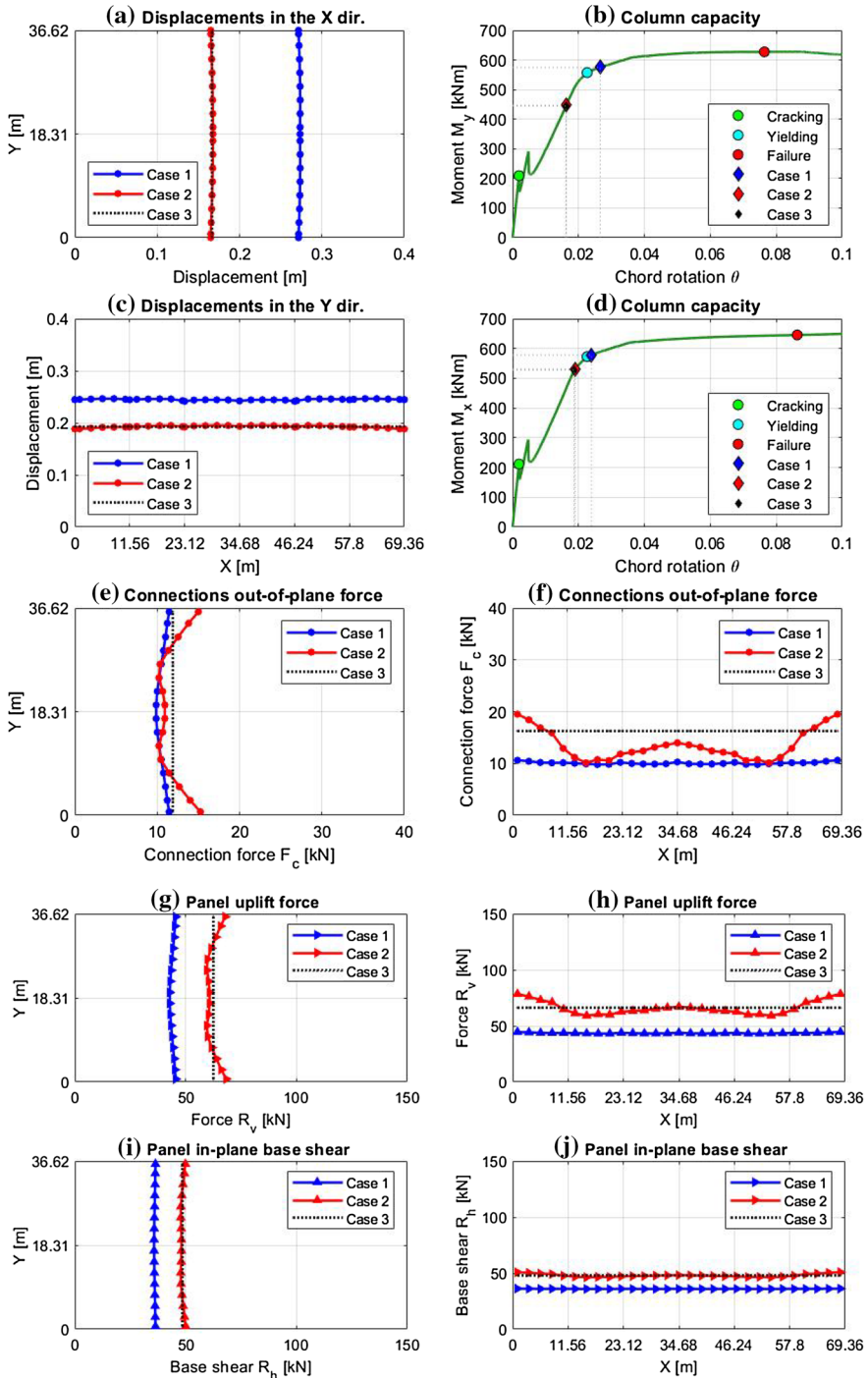


Fig. 23 Results for the L'Aquila earthquake

Emilia Earthquake 1st shock May 20, 2012

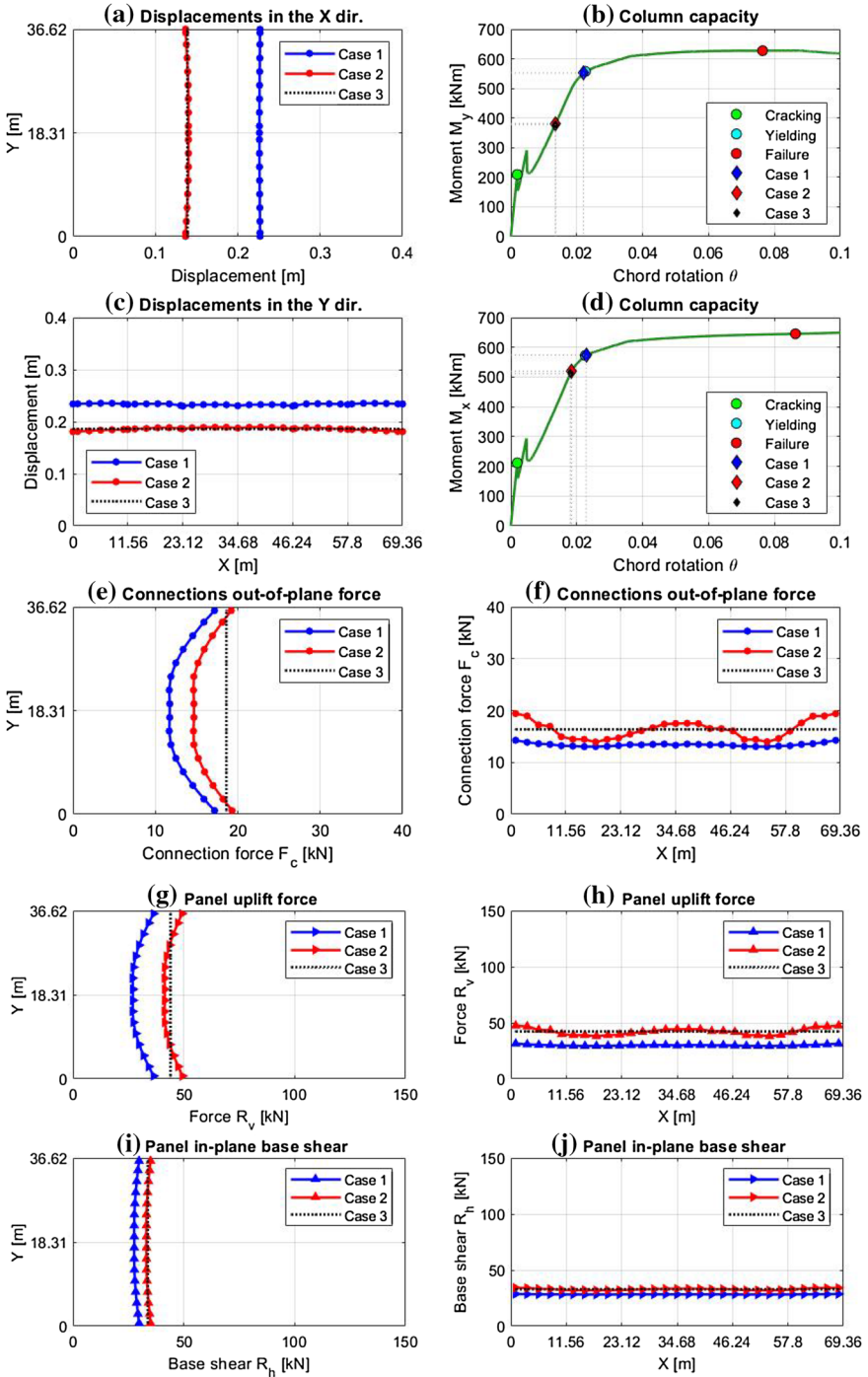


Fig. 24 Results for the Emilia 1st shock earthquake

Norcia Earthquake Oct. 30, 2016

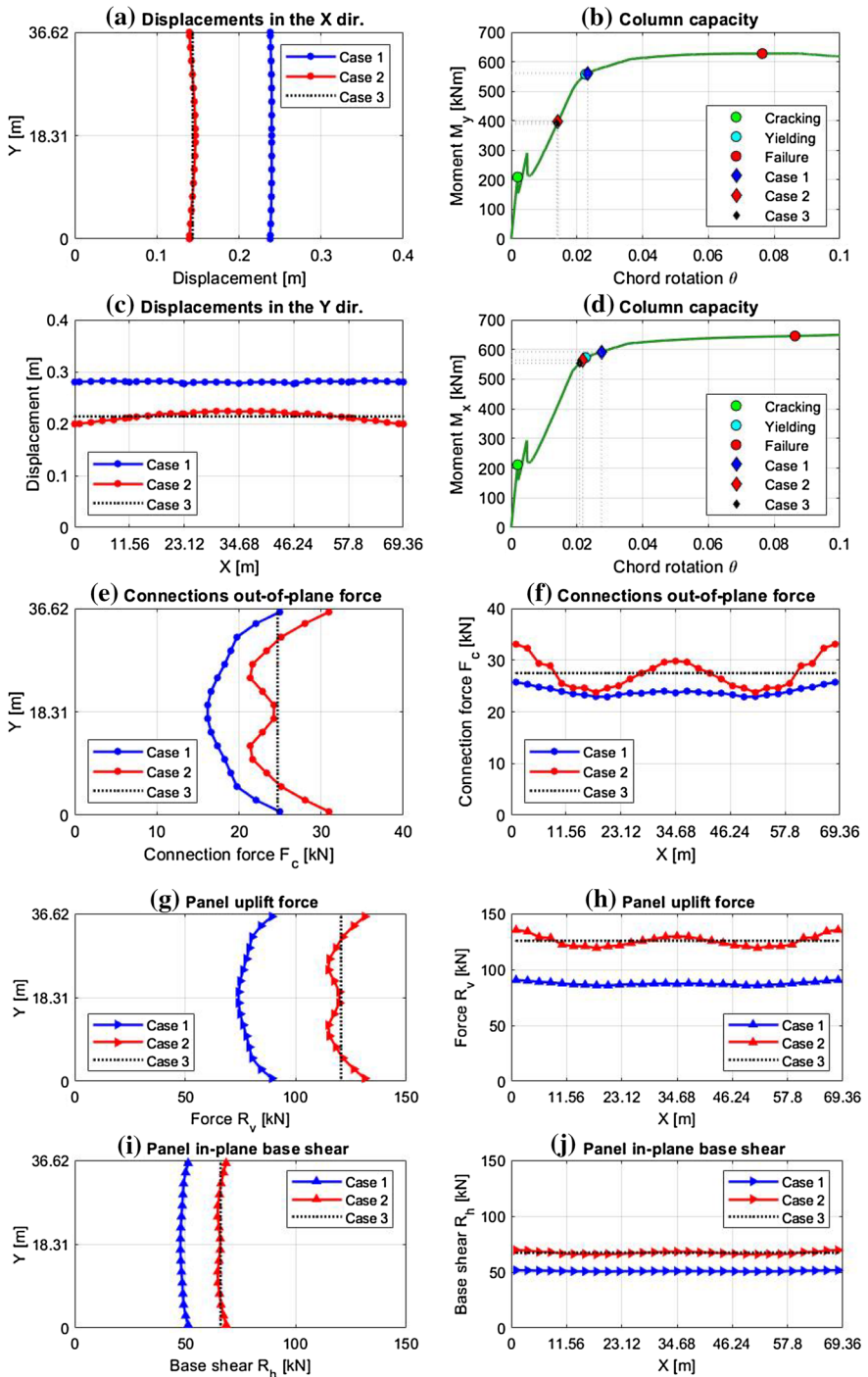


Fig. 25 Results for the Norcia earthquake

Emilia Earthquake 2nd shock May 29, 2012

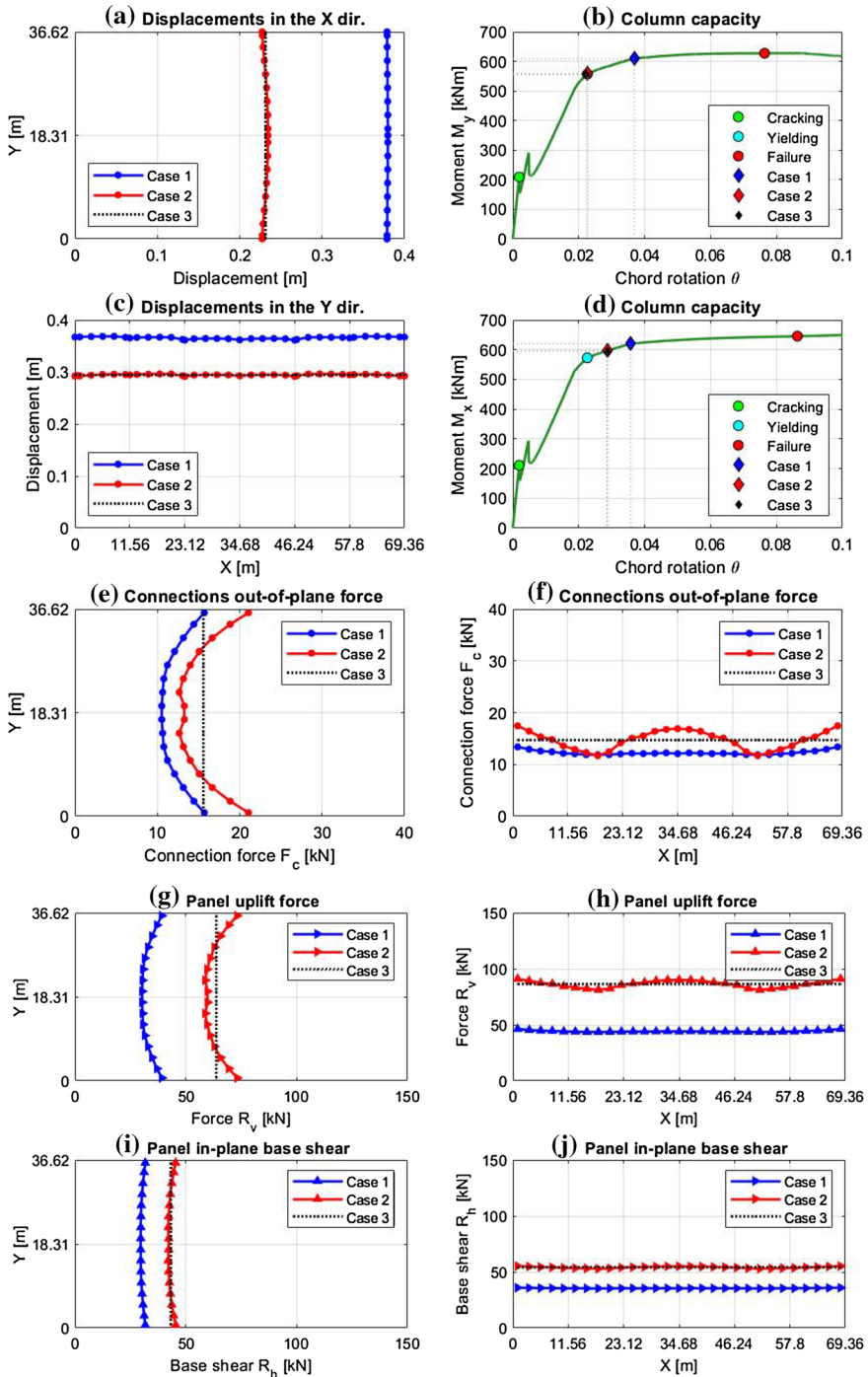


Fig. 26 Results for the Emilia 2nd shock earthquake

Table 7 Structure displacement for Case 1, 2 and 3 and percentage differences compared to Case 3

Case study	Seismic event							
	L'Aquila		Emilia 1st shock		Norcia		Emilia 2nd shock	
<i>Case 1</i>								
X displ (m)								
Max	0.273	63.5%	0.227	65.7%	0.240	66.7%	0.380	63.8%
Min	0.271	62.3%	0.225	64.2%	0.238	65.3%	0.378	62.9%
Mean	0.272	62.9%	0.226	65.0%	0.239	66.0%	0.379	63.4%
Y displ (m)								
Max	0.246	26.8%	0.235	27.7%	0.282	31.8%	0.368	24.7%
Min	0.241	24.2%	0.230	25.0%	0.276	29.0%	0.361	22.4%
Mean	0.244	25.8%	0.233	26.6%	0.280	30.8%	0.365	23.7%
<i>Case 2</i>								
X displ (m)								
Max	0.168	0.6%	0.140	2.2%	0.146	1.4%	0.234	0.9%
Min	0.164	-1.8%	0.136	-0.7%	0.139	-3.5%	0.227	-2.2%
Mean	0.166	-0.6%	0.138	0.7%	0.143	-0.7%	0.231	-0.4%
Y displ (m)								
Max	0.195	0.5%	0.190	3.3%	0.224	4.7%	0.296	0.3%
Min	0.188	-3.1%	0.181	-1.6%	0.199	-7.0%	0.291	-1.4%
Mean	0.192	-1.0%	0.186	1.1%	0.213	-0.5%	0.294	-0.3%
<i>Case 3</i>								
X displ (m)								
Mean	0.167		0.137		0.144		0.232	
Y displ (m)								
Mean	0.194		0.184		0.214		0.295	

which the top of panels is fixed. For panels lying in the longitudinal X direction, a longitudinal beam with the flexural stiffness of the edge main beam (1 or 3 in Fig. 27) can be considered. Those beams are supported on springs with stiffness K_{ix} or K_{iy} , which are equal to the translational stiffness of frames in the considered direction: three equal springs in the X direction ($K_{1x} = K_{2x} = K_{3x}$) and seven equal springs in the Y direction ($K_{Ay} = K_{By} = \dots = K_{Gy}$). Moreover, in the horizontal x-y plane the rotations of the three supported sections of the equivalent transversal beam are neglected (see the qualitative deformed configuration of the roof in the longitudinal direction in.

Figure 15a); this hypothesis derives from the much higher bending stiffness in the horizontal plane of main beams compared to roof beams.

The tributary masses of each frame in the considered direction are applied on the beam. The masses of the panels are connected to the beam through springs whose stiffness k_c is given by the out-of-plane stiffness of connections. In the equivalent beam schematization, half of the mass of each panel ($m_p/2$) was considered. All masses were calculated using uniform loads described in Sect. 3.1 and their values are provided in Table 9 with reference to tributary areas shown in Fig. 27. Then the mass and stiffness values used in the equivalent beam schematization are listed in Table 10.

Table 8 Out-of-plane forces for Case 1, 2 and 3 and percentage differences compared to Case 3

Case study	Seismic event							
	L'Aquila		Emilia 1st shock		Norcia		Emilia 2nd shock	
<i>Case 1</i>								
X dir. (kN)								
Max	11.45	-4.2%	17.19	6.0%	24.96	0.8%	15.70	0.4%
Min	9.88	-17.3%	11.68	-28.0%	16.18	-34.6%	10.54	-32.6%
Mean	10.63	-11.0%	13.60	-16.1%	19.27	-22.1%	12.32	-21.2%
Y dir (kN)								
Max	10.64	-21.7%	14.27	-13.2%	25.73	-6.5%	13.40	-9.1%
Min	9.82	-27.8%	13.04	-20.6%	22.89	-16.8%	11.87	-19.4%
Mean	10.10	-25.7%	13.42	-18.3%	23.93	-13.0%	12.28	-16.6%
<i>Case 2</i>								
X dir. (kN)								
Max	15.25	27.6%	19.31	19.0%	30.95	25.0%	21.05	34.6%
Min	10.20	-14.7%	14.63	-9.8%	21.36	-13.7%	12.66	-19.1%
Mean	11.91	-0.4%	16.19	-0.2%	24.70	-0.2%	15.59	-0.3%
Y dir (kN)								
Max	19.53	43.7%	19.41	18.2%	33.09	20.3%	17.46	18.5%
Min	10.12	-25.5%	13.93	-15.2%	23.74	-13.7%	11.71	-20.5%
Mean	13.56	-0.2%	16.38	-0.3%	27.49	-0.1%	14.72	-0.1%
<i>Case 3</i>								
X dir. (kN)								
Mean	11.95		16.22		24.75		15.64	
Y displ (m)								
Mean	13.59		16.43		27.51		14.73	

When the beam is subjected to the earthquake acceleration, its response is a function of the frame stiffnesses K_x and K_y , of the participating masses m_j and m_i and of the frequency content of the applied excitation, which can make half of the mass of each panel $m_p/2$ to respond in phase or in counterphase with masses m_j and m_i of frames. However, when the connection frictional behavior is taken into account, the stiffnesses K_{Ay} and K_{Gy} of the two edge frames in the Y direction and the stiffnesses K_{1x} and K_{3x} of the two edge frames in the X direction increase significantly compared to Case 1, because the displacement of edge frames is reduced by the friction forces transmitted by the cladding panels. That assumption requires to check the in-plane resistance of the base connection of panels, otherwise, the stiffening effect of panels could not be considered. To this aim, in Sect. 3.6 the resistance verification of the base connection is dealt with.

In Case 2, due to the increase of the translational stiffness of edge frames, the displacement of the end joints of the equivalent beam decreases, so the connections close to the edge frames are subjected to higher out-of-plane forces than the other connections.

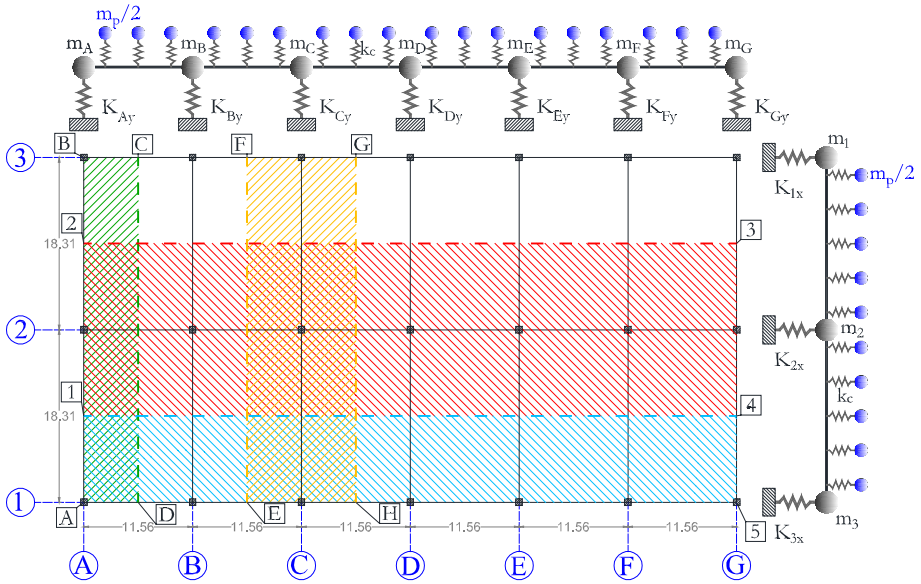


Fig. 27 Schematization with spring supported beams and tributary areas for mass calculation (each vertex is marked with a capital letter inscribed in a square)

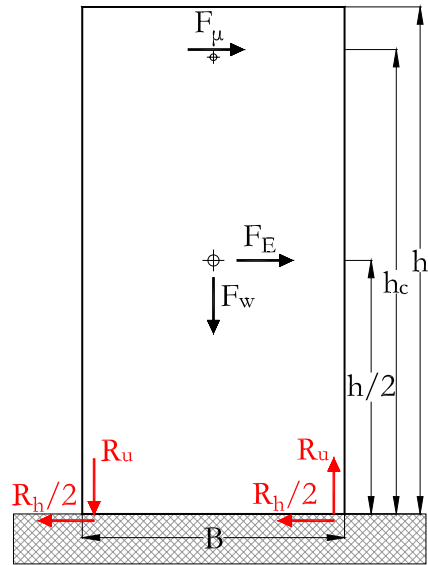
Table 9 Computation of masses and relative tributary areas

Tributary area (Fig. 27)	Mass m_A (kg s ² /m)	Mass m_C (kg s ² /m)	Mass m_3 (kg s ² /m)	Mass m_2 (kg s ² /m)
	ABCD	EFGH	A145	1234
Roof elements	2006.60	4013.19	6019.79	12,039.58
Vault shell elements	222.24	444.47	666.71	1333.42
Super dead	237.34	474.68	712.02	1424.04
Columns	1370.18	1370.18	3197.09	3197.09
Beams	1490.66	2981.33	5302.75	7282.45
Total	5327.02	9283.85	15,898.36	25,276.57

Table 10 Equivalent beam parameters

Equivalent beam parameters		
$m_p/2$	440.52	kg s ² /m
$m_1 = m_3$	15,898.36	kg s ² /m
m_2	25,276.57	kg s ² /m
$m_A = m_G$	5327.02	kg s ² /m
$m_B = m_C = m_D = m_E = m_F$	9283.85	kg s ² /m
K_{ix}	6319	kN/m
K_{iy}	2708	kN/m
k_c	5357	kN/m

Fig. 28 Forces acting on the panel for seismic force to the right: F_μ friction force transmitted by the panel-to-structure connection (due to a relative displacement of the structure to the right), F_E inertial force of the panel, F_w dead weight of the panel, R_h and R_v horizontal and vertical reaction of fixing devices



3.6 In-plane forces at the base of panels

Panels are fully-fixed at the base, that is they are equipped with connection devices capable of preventing the panel rocking and horizontal sliding, so they can withstand the uplifting reaction force R_v and the shear reaction force R_h shown in Fig. 28.

The connection devices at the top of the panel, which develop a friction force F_μ , increase the demand for both the uplifting force R_v and the shear force R_h . Those reaction forces can be evaluated through the equilibrium of the forces acting on the panel (Dal Lago et al. 2012). The reaction shear force R_h can be calculated by imposing the translational equilibrium of the panel:

$$R_h(t) = F_\mu(t) + F_E(t) - R_f \tag{2}$$

where F_μ , defined in the Eq. 1, is the friction force that develops in the connection device at the top of the panel and is equal to the out-of-plane force F_c of the connection multiplied by the friction coefficient μ .

F_E is the horizontal force imposed by the earthquake equal to the mass of the panel m_p multiplied by the seismic acceleration a_E :

$$F_E(t) = m_p \cdot a_E(t) \tag{3}$$

R_f is the friction force at the base of the panel, which in safety could be neglected; in any case it should be taken not higher than the weight force F_w multiplied by the static friction coefficient of concrete-to-concrete μ_{cc} (typically equal to 0.65):

$$R_f \leq \mu_{cc} \cdot F_w \tag{4}$$

With reference to Figs. 23, 24, 25, 26i and l, Table 11 lists the maximum, minimum and mean shear force R_h at the base of panels and the percentage difference compared to Case

Table 11 Mean shear forces for Case 1, 2 and 3 and percentage differences compared to Case 3

Case study	Seismic event							
	L'Aquila		Emilia 1st shock		NorciaNorcia		Emilia 2nd shock	
<i>Case 1</i>								
X dir. (kN)								
Max	36.40	-17.8%	36.38	-17.5%	89.21	-26.2%	39.19	-38.8%
Min	35.77	-19.2%	26.92	-39.0%	74.14	-38.7%	30.32	-52.6%
Mean	36.07	-18.6%	30.22	-31.5%	79.45	-34.3%	33.38	-47.8%
Y dir (kN)								
Max	36.23	-9.9%	31.42	-26.0%	90.54	-28.1%	46.19	-46.7%
Min	35.90	-10.7%	29.31	-30.9%	85.67	-32.0%	43.57	-49.7%
Mean	36.02	-10.5%	29.96	-29.4%	87.46	-30.6%	44.27	-48.9%
<i>Case 2</i>								
X dir. (kN)								
Max	45.46	2.7%	49.36	11.9%	131.21	8.5%	73.16	14.3%
Min	43.44	-1.9%	41.32	-6.3%	114.75	-5.1%	58.75	-8.2%
Mean	44.13	-0.4%	44.01	-0.2%	120.48	-0.3%	63.79	-0.3%
Y dir (kN)								
Max	42.39	5.4%	47.50	11.9%	135.27	7.4%	91.04	5.1%
Min	38.63	-4.0%	38.09	-10.2%	119.23	-5.3%	81.17	-6.3%
Mean	40.01	-0.5%	42.29	-0.3%	125.65	-0.2%	86.34	-0.3%
<i>Case 3</i>								
X dir. (kN)								
Mean	44.29		44.12		120.88		63.99	
Y displ (m)								
Mean	40.22		42.43		125.95		86.64	

3. For Case 3, since the roof is supposed to behave like a rigid diaphragm, the maximum, minimum and mean values of R_h are the same, so only the latter is reported in Table 11.

The uplifting force R_v can be calculated by imposing the equilibrium on the rotation for the panel in which F_μ and F_c are overturning forces while the weight force F_w is the stabilizing force.

$$R_v = \left[F_\mu(t) \cdot h_c + F_E(t) \cdot \frac{h}{2} - F_w \cdot \frac{B}{2} \right] \cdot \frac{1}{B} \tag{5}$$

where:

$$F_w = m_p \cdot g \tag{6}$$

is the weight force, equal to the mass of the panel m_p multiplied by the acceleration of gravity g , h is the total height of the panel, h_c is the height of the top connection above the panel base, and B is the panel width.

By looking at the graphs in Figs. 23, 24, 25, 26g, h, i and l, it can be noticed that the trend of the forces R_v and R_h has the same shape as the out-of-plane force F_c on the connections. This is due to both the proportionality between F_μ and F_c and the constant value of forces F_w (weight) and F_E (earthquake) for all panels. As for F_c , it is noted that the

Table 12 Mean uplift forces for Case 1, 2 and 3 and percentage differences compared to Case 3

Case study	Seismic event							
	L'Aquila		Emilia 1st shock		Norcia		Emilia 2nd shock	
<i>Case 1</i>								
X dir. (kN)								
Max	45.55	-27.4%	17.19	6.0%	24.96	0.8%	15.70	0.4%
Min	42.85	-31.7%	11.68	-28.0%	16.18	-34.6%	10.54	-32.6%
Mean	44.15	-29.6%	13.60	-16.1%	19.27	-22.1%	12.32	-21.2%
Y dir (kN)								
Max	44.51	-19.6%	14.27	-13.2%	25.73	-6.5%	13.40	-9.1%
Min	43.09	-22.1%	13.04	-20.6%	22.89	-16.8%	11.87	-19.4%
Mean	43.57	-21.3%	13.42	-18.3%	23.93	-13.0%	12.28	-16.6%
<i>Case 2</i>								
X dir. (kN)								
Max	68.27	8.8%	19.31	19.0%	30.95	25.0%	21.05	34.6%
Min	59.59	-5.0%	14.63	-9.8%	21.36	-13.7%	12.66	-19.1%
Mean	62.53	-0.3%	16.19	-0.2%	24.70	-0.2%	15.59	-0.3%
Y dir (kN)								
Max	65.35	18.1%	19.41	18.2%	33.09	20.3%	17.46	18.5%
Min	49.20	-11.1%	13.93	-15.2%	23.74	-13.7%	11.71	-20.5%
Mean	55.10	-0.4%	16.38	-0.3%	27.49	-0.1%	14.72	-0.1%
<i>Case 3</i>								
X dir. (kN)								
Mean	62.73		16.22		24.75		15.64	
Y displ (m)								
Mean	55.33		16.43		27.51		14.73	

values of R_v and R_h increase at the panels closest to the edge of the building. Table 12 lists the maximum, minimum, mean uplift force value R_v at the panels' base and the percentage difference with Case 3. Again, for Case 3, since the roof behaves like a rigid diaphragm, the maximum, minimum, R_v force are the same and only the latter is reported in Table 12.

4 Conclusions

The out-of-plane capacity of isostatic panel-to-structure connections of one-story precast structures was investigated through experimental tests. The experimental campaign consisted of 30 tests on two different typologies of mechanical connections, one typology was chosen among available in-use commercial joints and the other one was designed by the authors. The first is the typical hammer-head steel strap, the second is made of a mobile guide which can slide along a fixed guide rail.

Under in-plane seismic forces, isostatic connections should be able to accommodate high relative displacements between the panels and the structure, therefore, it is important to test and evaluate their displacement capability. Under out-of-plane seismic forces, the connections should have a satisfactory out-of-plane resistance and restrain out-of-plane

relative displacements between the cladding panels and the structure to preserve the structural integrity. The experimental tests allowed to evaluate the capacity of the studied devices for out-of-plane forces both on the beam side and on the panel side. The lesser between the two resistances is always given by the connection on the panel side, which represents the ultimate resistance of the device.

The tests highlighted that the Standard devices have a lower out-of-plane resistance than the SismoSafe devices: on the panel side they exhibited an ultimate resistance about three times lower than SismoSafe connections under both cyclic and monotonic load. Moreover, the actual capacity of Standard connections is even lower than the experimental one, as they are damaged by in-plane seismic forces, as already highlighted in a previous research by the same authors. The SismoSafe devices do not suffer damage due to relative in-plane displacements, so the experimental out-of-plane capacity could be considered reliable.

A series of non-linear dynamic analyses were also carried out to evaluate the out-of-plane forces in the SismoSafe panel-to-structure connections of a one-story industrial building, considering the four strongest Italian earthquakes of the last 12 years. Numerical results confirmed that the new SismoSafe connections could safely withstand the out-of-plane forces for all the four seismic events whether the in-plane friction force is considered or not. The numerical analyses allowed to highlight the influence of friction at the connections on the seismic response of the structure. At increasing the friction force, the uplift and shear reaction forces at the base of panels parallel to the earthquake direction increase, as well as the out-of-plane forces at the top of panels normal to the earthquake. Therefore, a very low friction is preferable, even if the friction at panel-to-structure could be beneficial to reduce the seismic displacements of the main structure. Nevertheless, the manufacturing of low friction devices could be very expensive and not convenient for industrial production.

The effect of friction is very pronounced on the panel-to-structure connections arranged along the transversal edge of the building. Here the panels are connected to the edge roof beam, which has a rather large span and great flexibility, so the out-of-plane forces on those connections due to longitudinal seismic loading have a very pronounced non-uniform distribution, much more than connections of panels fixed to the edge longitudinal beams for transversal seismic loading. Vice versa, in one-story precast buildings with a rigid diaphragm roofing system, the distribution of out-of-plane forces on the connections is uniform without peaks at the edge frames.

Traditional panel-to-structure connections made with hammer-head strap devices could not withstand the demand for out-of-plane force and in-plane displacement required by those four seismic events. The hammer-head strap devices have a limited in-plane displacement capacity for available on the market devices and a limited out-of-plane capacity (≈ 15 kN). Furthermore, during a seismic event, they are susceptible to in-plane damage, which could reduce significantly the out-of-plane capacity of the standard connections. On the contrary, the SismoSafe devices, even if they transmit in-plane friction forces, can sustain very large displacements in the plane, which depend on the length of the fixed guide inside which the mobile cursor slides. The out-of-plane resistance capacity of the SismoSafe devices is about 45 kN, as evaluated through the experimental campaign, so the number of devices required to withstand the out-of-plane seismic actions is three times lower than standard connections. In none of the four considered seismic events, the in-plane displacement capacity, as well as the out-of-plane resistance capacity, were never exceeded. Moreover, the out-of-plane resistance of the SismoSafe connections is not affected by the in-plane sliding behavior, so they could work correctly even in the presence of randomly inclined seismic actions.

Acknowledgements The authors would like to thank the Company Baraclit S.p.A., who commissioned the experimental campaign and provided specimens and technical support. The authors also thank the Structures and Materials Testing Laboratory (SMTS) team of the Department of Civil and Environmental Engineering in Florence, Mr. Saverio Giordano, Mr. Franco Bruni and Mr. Enzo Barlacchi and Spin-Off S2R team for their support during all the phases of the experimental campaign.

Funding Open access funding provided by Università degli Studi di Firenze within the CRUI-CARE Agreement.

Open Access This article is licensed under a Creative Commons Attribution 4.0 International License, which permits use, sharing, adaptation, distribution and reproduction in any medium or format, as long as you give appropriate credit to the original author(s) and the source, provide a link to the Creative Commons licence, and indicate if changes were made. The images or other third party material in this article are included in the article's Creative Commons licence, unless indicated otherwise in a credit line to the material. If material is not included in the article's Creative Commons licence and your intended use is not permitted by statutory regulation or exceeds the permitted use, you will need to obtain permission directly from the copyright holder. To view a copy of this licence, visit <http://creativecommons.org/licenses/by/4.0/>.

References

- Arnold C (1989) Cladding design: recent architectural trends and their impact on seismic design. In: International symposium on architectural precast concrete cladding—its contribution to lateral resistance of buildings, Chicago
- Baird A, Diaferia R, Palermo A, Pampanin S (2011) Parametric investigation of seismic interaction between precast concrete cladding systems and moment resisting frames. *Struct Congr* 2011:1286–1297
- Belleri A, Cornali F, Passoni C, Marini A, Riva P (2018) Evaluation of out-of-plane seismic performance of column-to-column precast concrete cladding panels in one-storey industrial buildings. *Earthq Eng Struct Dyn* 47(2):397–417
- Belletti B, Gasperi A, Spagnoli A (2015) Capacity design-based seismic forces in floor-to-beam connections of precast concrete frames. *J Perform Construct Facil* 29(6):4014161. [https://doi.org/10.1061/\(ASCE\)CF.1943-5509.0000649](https://doi.org/10.1061/(ASCE)CF.1943-5509.0000649)
- Biondini F, Dal Lago BA, Toniolo G (2013) Role of wall panel connections on the seismic performance of precast structures. *Bull Earthq Eng* 11:1061–1081. <https://doi.org/10.1007/s10518-012-9418-z>
- Brunesi E, Nascimbene R, Bolognini D, Bellotti D (2015) Concrete framed structures. *PCI J* 60:57–79
- Burley J, Faitotoa T, Seifi P, Henry RS, Ingham JM (2014) Out-of-plane behaviour of connections between precast concrete panels and their foundations. In: Proceedings of the New Zealand concrete industry conference, Wairakei, New Zealand, October, 9–11
- Burridge SM, Casey MP, Raby ML, Wright HD, Hogan L, Henry RS, Ingham JM (2015) Improved detailing of precast concrete panel to foundation connections to withstand out-of-plane earthquake loads. In: The New Zealand concrete industry conference, Rotorua, New Zealand
- Colombo A, Toniolo G, Lamperti M, Negro P (2016) Design guidelines for precast structures with cladding panels. JRC Technical report
- Dal Lago BA, Lamperti Tornaghi M, Dal Lago A (2012) Studio sul comportamento bidirezionale di connessioni meccaniche scorrevoli pannello-telaio. In: 19° Convegno CTE, pp 31–140
- Dal Lago BA, Toniolo G, Lamperti Tornaghi M (2016) Influence of different mechanical column-foundation connection devices on the seismic behaviour of precast structures. *Bull Earthq Eng* 14(12):3485–3508. <https://doi.org/10.1007/s10518-016-0010-9>
- Dal Lago BA, Biondini F, Toniolo G (2018) Experimental Investigation on steel W-shaped folded plate dissipative connectors for horizontal precast concrete cladding panels. *J Earthq Eng* 22(5):778–800. <https://doi.org/10.1080/13632469.2016.1264333>
- Del Monte E, Falsini C, Boschi S, Menichini G, Orlando M (2019) An innovative cladding panel connection for RC precast buildings. *Bull Earthq Eng* 17(2):845–865. <https://doi.org/10.1007/s10518-018-0470-1>
- EN 1992-1-1 (2004) Eurocode 2: design of concrete structures. Part 1-1: General rules and rules for buildings
- EN 1998-1-1 (2005) Eurocode 8: design of structures for earthquake resistance. Part 1: general rules, seismic actions and rules for buildings
- Ercolino M, Magliulo G, Manfredi G (2016) Failure of a precast RC building due to Emilia-Romagna earthquakes. *Eng Struct* 118:262–273

- Fischinger M, Zoubek B, Isaković T (2014) Seismic response of precast industrial buildings. In: *Perspectives on European earthquake engineering and seismology*. Springer, Cham, pp 131–177
- Goodno BJ, Craig J (1989) Historical overview of studies on the contribution of cladding to lateral resistance of buildings. In: *Architectural precast concrete cladding—its contribution to lateral resistance of buildings*, pp 36–47
- IBC (2018) International Building Code. International Code Council, USA
- Liberatore L, Sorrentino L, Liberatore D, Decanini LD (2013) Failure of industrial structures induced by the Emilia (Italy) 2012 earthquakes. *Eng Fail Anal* 34:629–647. <https://doi.org/10.1016/j.engfailana.1.2013.02.009>
- Luzi L, Pacor F, Puglia R (2019) Italian Accelerometric Archive v 3.0 Istituto Nazionale di Geofisica e Vulcanologia, Dipartimento della Protezione Civile Nazionale. <https://doi.org/10.13127/itaca.3.0>
- Magliulo G, Ercolino M, Petrone C, Coppola O, Manfredi G (2014) The Emilia earthquake: seismic performance of precast reinforced concrete buildings. *Earthq Spectra* 30(2):891–912. <https://doi.org/10.1193/091012EQS285M>
- Magliulo G, Ercolino M, Manfredi G (2015) Influence of cladding panels on the first period of one-story precast buildings. *Bull Earthq Eng* 13(5):1531–1555. <https://doi.org/10.1007/s10518-014-9657-2>
- Mandelli Contegni M, Palermo A, Toniolo G (2007) Strutture prefabbricate: schedario dei collegamenti. Italian Civil Protection Department, ReLUIS and Assobeton
- Mander BJ, Priestley NMJ, Park R (1988) Theoretical stress–strain model for confined concrete. *J Struct Eng* 114(8):1804–1826. [https://doi.org/10.1061/\(ASCE\)0733-9445\(1988\)114:8\(1804\)](https://doi.org/10.1061/(ASCE)0733-9445(1988)114:8(1804))
- Mazzoni S, McKenna F, Scott MH, Fenves GL (2006) OpenSees: a framework for Earthquake engineering simulation. Pacific Earthquake Engineering Research (PEER) Center. Retrieved from <https://opensees.berkeley.edu/>
- Orlando M, Piscitelli LR (2018) Experimental investigation on static and cyclic behaviour of flanged unions for precast reinforced concrete columns. *Eur J Environ Civ Eng* 22(8):927–945. <https://doi.org/10.1080/19648189.2016.1229226>
- Savoia M, Buratti N, Vincenzi L (2017) Damage and collapses in industrial precast buildings after the 2012 Emilia earthquake. *Eng Struct* 137:162–180. <https://doi.org/10.1016/j.engstruct.2017.01.059>
- Toniolo G, Colombo A (2012) Precast concrete structures: the lessons learned from the L'Aquila earthquake. *Struct Concrete* 13(2):73–83. <https://doi.org/10.1002/suco.201100052>
- Zoubek B, Fischinger M, Isaković T (2016) Cyclic response of hammer-head strap cladding-to-structure connections used in RC precast building. *Eng Struct* 119:135–148. <https://doi.org/10.1016/j.engstruct.2016.04.002>
- Zoubek B, Fischinger M, Isaković T (2018) Seismic response of short restrainers used to protect cladding panels in RC precast buildings. *J Vib Control* 24(4):645–658. <https://doi.org/10.1177/1077546316659780>

Publisher's Note Springer Nature remains neutral with regard to jurisdictional claims in published maps and institutional affiliations.